Fretting wear in mechanical systems: innovative design and graphene-based improvements

ScuDo
Scuola di Dottorato ~ Doctoral School
WHAT YOU ARE, TAKES YOU FAR

Doctoral Dissertation
Doctoral Program in Mechanical Engineering (31st Cycle)

Fretting wear in mechanical systems: innovative design and graphene-based improvements

Federica Adamo
* * * * * *

Supervisor
Prof.ssa Francesca Maria Curà

Politecnico di Torino
July, 2019

I hereby declare that, the contents and organisation of this dissertation constitute my own original work and does not compromise in any way the rights of third parties, including those relating to the security of personal data.

Summary

The research activity is based on the study of the phenomenon of fretting wear in spline couplings from the theoretical, numerical and experimental point of view. The fretting wear occurring in mechanical systems when sliding parts are in contact, leading to surface damage. The mechanical components affected from fretting wear experience malfunction, noisiness and loss of efficiency. The most common model to describe the fretting phenomenon is called Archard law. Starting from the Archard law, the goal is the analysis of the main parameters influencing the fretting and the consequent individuation of their effect on the spline couplings. Basing on the Archard law the wear volume depends on: contact pressure, sliding and material properties. Through an iterative design process, based on the development of a dedicated FEM model, the micro-geometric parameters of the component directly related to the contact pressure value and distribution have been identified, such as the crowning radius and the tooth profile. Moreover, for the sliding, the main sources, as misalignment and variable torque have been described. In order to reduce the entity of the sliding, the effect of the variation of the tooth stiffness has been evaluated, by means a progressive reduction of its thickness. Continuing with the analysis of the Archard law parameters, the study focuses on the wear volume. Given the difficulty to estimate the amount of loss material, the evaluation of the wear volume in damaged spline couplings have been discussed: a method able to calculate it using a 2D profilometer and some mathematical assumptions have been presented. Moreover, the difficult to carry out experimental tests for spline coupling characterized by high dimension (as that for high power transmissions) make necessary to develop a way to predict the wear volume. Then, a method for the prediction, based on the use of a pin-on-disk tribometer have been developed and discussed. The last parameter involving on the Archard law is the wear coefficient that depends on the materials and on the lubrication conditions. In order to find solutions to mitigate friction and wear, a series of experimental tests have been developed on the dedicated test bench. The purpose of these tests is the measurement of the friction coefficient following the addition of Graphene Nano-Platelets (GNP) into the grease for spline couplings. A series of preliminary Pin-on-disk tests on three different greases have been carried out:

three different greases were added, using different percentages of GNP respectively. The results of both test bench test and pin-on-disk test confirm the good effect of graphene in reducing coefficient of friction. Finally, the possibility to use graphene as solid lubricants for steel have been investigated. For the production of the specimens, different techniques of graphene production and coating were used; the characterization of the surfaces following both the covering process and the tribological tests was carried in order to define the wear mechanisms affecting the surface. A series of pin-on-disk tests have been carried out confirming the possibility to use graphene as solid lubricant.

Ringraziamenti

Al termine di questo meraviglioso percorso di dottorato, l'emozione, la felicità, e la soddisfazione per aver raggiunto il traguardo non ha eguali. Ed è proprio in questo turbinio di emozioni che non posso esimermi dal ringraziare chi ha contribuito alla realizzazione di ciò. Infatti, essendo consapevole di quanto sia prezioso il sostegno e l'aiuto delle persone care, mi sento estremamente fortunata ad essere stata circondata in questi anni di lavoro da persone magnifiche verso le quali nutro profonda stima.

Più di 4 anni fa, ho avuto l'onore ed il privilegio di entrare a far parte del gruppo di ricerca del mio supervisor: la prof.ssa Francesca Curà. Lei, che è stata la prima a cogliere la mia volontà ed il mio entusiasmo nell'intraprendere questo cammino; lei, che con autorevolezza e dolcezza mi ha guidata lungo tutto il dottorato, aiutandomi, supportandomi, incoraggiandomi e facendomi sempre sentire all'altezza di qualsiasi situazione. Grazie, cara professoressa, per aver sempre creduto nelle mie capacità, per le innumerevoli volte in cui mi hai ascoltata, per gli infiniti insegnamenti trasmessimi, non solo di lavoro, ma anche di vita… li custodirò gelosamente.

Questi anni di lavoro al Politecnico non sarebbero stati gli stessi se al mio fianco non ci fosse stato il prof. Andrea Mura. Come un "fratello maggiore" mi ha accolta e seguita facendomi sentire parte integrante del gruppo. La profonda passione e pazienza con le quali svolge il suo lavoro sono state per me continua fonte di ammirazione ed il suo incredibile ingegno, la sua intelligenza e genialità continua fonte d'ispirazione. Ti sono grata per avermi dato la possibilità di lavorare con te, per essere stato un eccellente compagno di lavoro, per essere stato un sostegno durante i miei sfoghi e momenti di sconforto, per aver condiviso con me innumerevoli pranzi e pause caffè… ma anche, e soprattutto, per essere stato un Amico.

Torino, mi ha permesso di raggiungere i miei più importanti traguardi ed i ricordi legati agli anni vissuti in questa splendida città resteranno per me indelebili. Col passare degli anni ho incrociato le vite di tanta gente… alcune persone sono entrate ed uscite dalla mia vita velocemente, altre sono diventate presenze più costanti… e poche sono diventate amiche fidate. Il mio grazie va alle mie Amiche Simona ed Anna per essere state una presenza costante durante

questi anni. Grazie per le esperienze indimenticabili vissute insieme, per le serate spensierate e per le mille risate. Grazie per essere state la mia famiglia a Torino.

Giungere fin qui, a scrivere le mie ultime righe su questa tesi, ha richiesto tanto impegno e dedizione. Se ho solcato la linea del traguardo è solo grazie a Lui… il mio amato Raffaele, la persona più straordinaria che io abbia mai conosciuto. Mi hai condotta per mano sino a qui, mi hai donato il tuo tempo prezioso ed hai fatto in modo che le mie priorità diventassero le tue. Sei il mio punto di riferimento, il mio migliore amico, la mia spalla su cui piangere. Grazie per aver condiviso con me l'amore per la ricerca, la stessa ricerca che ci ha fatti incontrare. Grazie perché hai camminato accanto a me, ma in punta di piedi, lasciandomi sempre libera di scegliere il mio futuro. E soprattutto, grazie per avermi concesso il privilegio di starti accanto, non avrei potuto desiderare di meglio che Te.

I ringraziamenti non potranno mai bastare per coloro senza i quali la mia vita non avrebbe senso… la mia famiglia. La mia adorata sorella, Valentina… solare, astuta, intraprendete e risoluta. Sei il mio esempio, la mia grande Amica. Con te ho condiviso ogni istante della mia vita. Tu che sei stata sempre presente, anche a distanza. Mi hai confortata e sostenuta nei momenti peggiori, prendendo aerei all'improvviso per arrivare quanto prima da me! E poi Voi, papà e mamma… grazie perché avete sempre mostrato una fiducia cieca in me, sostenendomi in qualsiasi circostanza ed incoraggiandomi ad inseguire sempre i miei sogni. Avete saputo guidarmi con intelligenza, saggezza e discrezione. Mi avete insegnato ad essere coraggiosa, a non avere mai paura di nulla e ad andare oltre ai miei limiti. Siete stati la mia forza, il mio pilastro… sempre presenti, comprensivi ed amorevoli. Non avrei potuto desiderare genitori migliori di voi… e se oggi sono diventata quella che sono è solo merito vostro.

Contents

List of Figures

List of Tables

Introduction

Wear is one of the most important causes of noisiness, malfunction and low efficiency of mechanical systems. One of the sources of surface damage is the fretting wear. This phenomenon occurs when parts in contact slid between them of a small amplitude. Given the growing need to work with even more reliable mechanical components, it becomes of primary importance to mitigate the fretting wear affecting the mechanical components.

The research activity presented on this thesis aims to the analysis of the fretting wear affecting spline couplings. The fretting wear occurring between the teeth in contact represents, in fact, one of the most important causes of run out of spline couplings used in high power transmission systems.

During the last decades the fretting wear have been studied by several researchers. Basing on the theoretical and experimental evidences found on the past, the objective of the first chapter will be to give a general explanation about the fretting wear. As explained on the chapter, different wear regimes can affect the system leading to different wear damage. In order to know witch regime can concern the mechanical system analysed, it is of first importance to understand the differences between them. Moreover, it also important to consider that, depending on the type of wear, different type of wear can affect the surfaces. In order to understand the main differences among them the different wear mechanisms will be descripted. Regarding the modelling of the fretting wear, during the years different models have been presented. The most common is the Archard model; it has been used by different researchers thanks to the simplicity and adaptability to different situations. The Archard model and the parameters involving on it (contact pressure, sliding and wear coefficient) will be presented and analysed. The last paragraph of the chapter 1 concerns the literature review about the fretting wear on spline couplings. The main causes of fretting wear on spline couplings are principally related to the design and to the working conditions. The more recent works are focused on the prediction of the fretting wear of spline coupling by means numerical models and experimental test; it is a difficult issue because of the complexity of the phenomenon.

On the basis of the Archard law, on the second chapter a detailed analysis of the design parameters involving on the wear will be presented. The study is

based on the development of a FEM: the model regards a crowned spline coupling and will be validated by means of the hertzian theory. Thanks to the numerical model, the microgeometry parameters directly influencing the contact pressure established between the teeth in contact will be identified. Later, the analysis will focus on the second most important parameters influencing the fretting wear: the sliding. The explanation of the different sources of sliding between the teeth will be given. Basing on the numerical model the influence of the teeth flexibility on the sliding entity will be also evaluated. The last part of the second chapter concerns the wear volume calculation on damaged spline couplings: it is a complex issue and an easy method to estimate it will be presented. Finally, the problem of predicting wear in spline coupling a priori will be addressed presenting an innovative way to estimate it.

The wear coefficient is the third parameter involved on the Archard law. It depends on the characteristics of the materials in contact and it is influenced by the lubrication conditions established on the parts in contact. Given the great importance of this aspect, the third chapter will focus on the improvement of the lubrication of spline couplings. The objective of the chapter is to investigate the possibility to use graphene as liquid lubricant additive. First, a series of preliminarily experimental test conducted on a pin-on-disk machine will be presented. The investigation regards three different greases generally used in spline couplings. Following these results, the better mixture of grease and graphene is tested by means a dedicated test rig for spline couplings. Then, the results of this application will be presented and discussed.

The mitigation of the friction and wear can be achieved using not only liquid lubricants but also solid lubricants. Focusing on the development of innovative solid lubricants, the fourth chapter will discuss about the possibility to use graphene monolayer as solid lubricant for steel. After the description of two different covering mechanisms, the results of the pin-on-disk test on the steel with graphene specimens will be presented. Wear mechanisms, coefficient of friction and wear coefficient will be discussed.

1 Fretting wear in mechanical systems

1.1 The fretting phenomenon

Fretting is defined as the small amplitude oscillating movement which may occur between contacting components subjected to working conditions as cyclic loads, mechanical vibration, electromagnetic shocks and thermal cycling [1], [2]. The fretting may result in surface damage as particles detachment and rapid cracks nucleation and propagation. The first phenomenon is called fretting wear and consists in the progressive removal of material and the consequent debris production. Instead, the cracks growth caused by fretting is identified as fretting fatigue.

The fretting process has been found to be dependent on a large number of variables, explaining the complexity of the fretting process. The way in which surface is damaged during fretting depends strongly on the contact conditions (geometry, normal and tangential forces, displacement amplitude, vibrational frequency) establishing on the rubbing surfaces. During the years a wide analysis on the fretting conditions has been developed [2]-[5]. The first important result has been achieved by Vingsbo and Söderberg [6] that, basing on experimental observation and theoretical analysis, distinguished three fretting regimes:

1) stick regime;
2) mixed stick-slip regime;
3) gross slip regime.

The stick regime is related to *low damage fretting*: the surfaces are slightly damaged by wear and oxidation and fatigue cracks are absent. The phenomenon is governed by elastic deformation of the contact interfaces sticking at the contact centre. The friction coefficient fluctuates in the steady-state stage. The *mixed stick-slip* is characterized by the growth of cracks that may result in strongly reduced fatigue life, while wear and oxidations phenomena are limited. As a consequence, the surface damage mode is the *fretting fatigue.* In this stage some elasto-plastic deformation appears and the coefficient of friction still corresponds to the static value. In the *gross slip* regime the surfaces appear to be

damaged by wear and oxidation phenomena. In this regime the formation of debris is the critical factor: the materials particles accumulate among the contacting surfaces and forms oxide beds that modify the properties of the interfaces leading to improper performances of the mechanical components. *Fretting wear* is the main surface damage mode. In this stage, the slip occurs in the whole contact zone, strong plastic deformations occur and a transition from static to kinetic friction happens.

As a result of the study, Vingsbo and Sodeberg developed apposite fretting maps showing the relevant fretting regimes in function of two variables. The wear maps permit to identify the fretting regime affecting the rubbing surfaces when the contact parameters are known. As an example, Figure 1.1 reports the fretting map in terms of normal load and sliding amplitude in which the three regimes are highlighted.

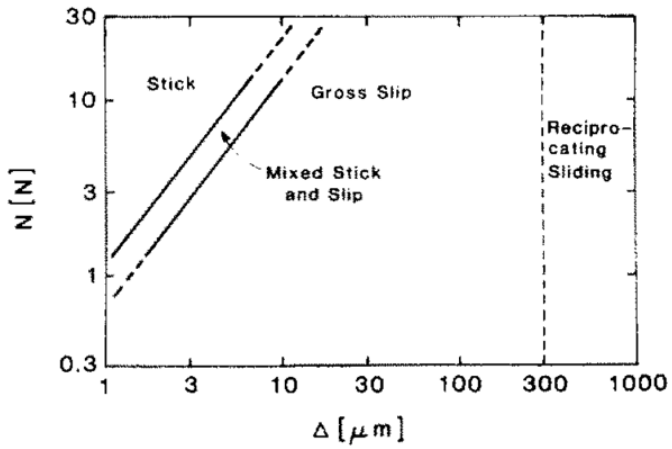

Figure 1.1. Wear map by Vingsbo [6].

The map shows the critical values of displacements amplitude defining the boundaries corresponding to each fretting regime. These values increasing linearly with normal load amplitude. Starting from a low amplitude case, an increase in the displacement amplitude determine the passage from the stick regime to the mixed stick slip regime: the risk of a fretting fatigue failure increases. A further increase on the displacement amplitude (above 10 μm about) would reduce the risk of fatigue failure at the expense of increased wear that characterized the gross slip regime. An explanation of this phenomenon was given by Nishioka and Hirakawa [7] demonstrating that, when the slip increases, the stress to initiate cracks becomes larger due to the abrasive effect of the wear that can abrade away previously initiated fretting fatigue cracks. At this point, an augmentation on the slip amplitude (above 300 μm) may inhibit the fretting process, when the reciprocating sliding regime appears.

1.2 Wear mechanisms

There are different wear mechanisms that can lead to the fretting wear. In order to analyse and, then, to prevent the wear on sliding systems, it is of fundamental importance to understand which of the existing wear mechanisms may result from certain contact conditions.

The main types of wear behaviour are [8]:

- adhesive wear;
- abrasive wear;
- corrosive wear;
- oxidative wear;
- thermal wear.

In general, during the sliding the surfaces are in contact between their asperities. The relative movement causes stress on the asperities and, after some cycles, their break with the production of new ones. The produced fragments are usually removed from the softer asperity and adhere to the harder surface forming a "transfer film" (see schematization on Figure 1.2). They can subsequently become loose and give rise to wear debris. This phenomenon is called *adhesive wear*. In this case, the fracture of the asperities can be ductile or brittle. Sometimes the adhesive wear is caused by the breakdown of the lubricant film, as for example in lubricated mechanical components that may experience starvation of lubricant [9].

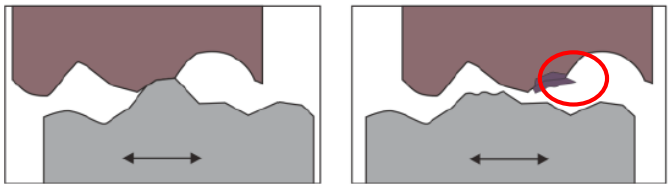

Figure 1.2. Adhesive wear schematization.

In the case of plastic contact between hard and sharp material and relatively soft material, the harder material penetrates to the softer one. When the fracture is supposed to be brought about in the manner of micro-cutting by the indented material, the resultant wear is called *abrasive wear.* The wear scar can be produced by an asperity of the harder material (two-body abrasive wear, figure) or by the hard particles confined between the surfaces (three-body abrasive wear, Figure 1.3). Such particles may be introduced between the two softer surfaces as a contaminant from the outside environment, or they may have been formed in situ by oxidation or by some other chemical or mechanical process. The surfaces affected by abrasive wear is characterized by scratching and long parallel grooves on the same direction of the sliding.

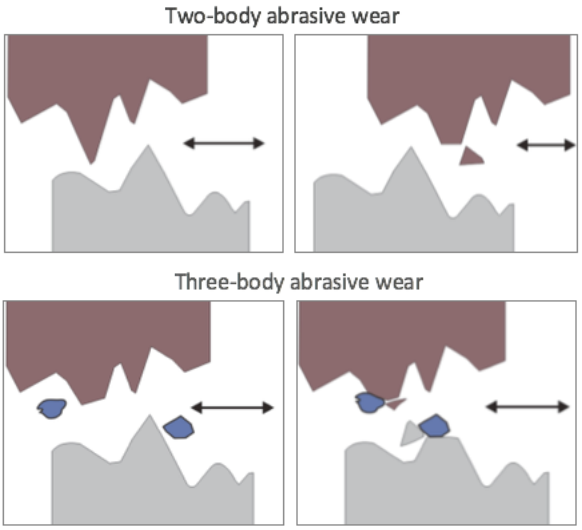

Figure 1.3. Abrasive wear schematization.

There are also other aspects to consider: during the sliding process some kind of interaction will occur between the environment and the surfaces in contact. As a consequence, in case of sliding contact in corrosive environment *corrosive wear* can occurs. When corrosion wear is combined with adhesive wear or abrasive wear, the wear rate can increase quickly. Chemical reactions of the surface with a chemical reagent or a reactive lubricant produce a film on the sliding surface. This film will be broken during the sliding by an adhesive or abrasive mechanism exposing fresh material to a new chemical reaction.

Moreover, on the most common case, if in the atmosphere oxygen is present a form of corrosive wear called *oxidative wear* can be exists. In Figure 1.4 a schematization of the mechanism is shown. Although the most part of the observation about oxidative wear regards steel sliding systems [10]-[12] more recently evidence of oxidative wear in aluminium alloys [13] and in magnesium alloys [14], [15] have been found.

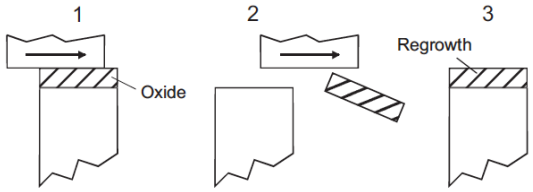

Figure 1.4. Oxidative wear schematization.

In other situations, the material removal can be governed by surface melting produced by frictional heating or by surface cracking caused by thermal stress. This wear mechanism is called *thermal wear*. Here the heat caused by the friction and partial high temperature governs the phenomenon.

In general, the different wear mechanisms don't take place alone, but often they coexist and interact. Analysing the worn surfaces, it is probable to find evidence that different mechanisms occurred. In fact, the different wear types can arise at different times or they could be related to the variation of the contact conditions during the sliding.

1.3 Archard Model

Many models developed for the description of the wear phenomenon are available in the literature. Their mathematical expressions vary from simple empirical relationships to complex equations based on physical concepts and principles [16]. The empirical equations are directly constructed on the basis of data taken from specific tests, then they are valid only within the range of the test as well as the parameters and variables involved. As a consequence, very few of those models have been used to predict wear in practice. The most frequently used wear model derives from contact-mechanics theory and it is known as the Archard wear law [17]. The basic form of the model was first published by Holm [18]. The equation was based on experimental observations and expresses the wear volume (V) as function of the most important parameters involving on the fretting phenomenon: the coefficients related to the materials (K and H), the load applied (F) and the sliding amplitude (S):

$$V = \frac{K\,F\,S}{H}$$

The parameter K is an empirical non-dimensional coefficient associated to the probability that during the contact between the rolling surfaces two asperity will produce a wear particle; while H is the penetration hardness of the softer material. The terms K and H are both related to the material response, then they can be grouped in a single parameter defined wear coefficient k. Using this notation, the equation becomes the follow:

$$V = k\,F\,S$$

During the years, the Archard model found application in many studies. Several others models related to particular applications have been derived from the Archard law, as the model for the percussive impact [19] or the Bayer zero model [20]. Goryacheva et al. [21] developed an analytical method to evaluate fretting wear under partial slip conditions starting from the Archard model. In 1994, Johansson [22] implemented the Archard law into an algorithm for the prediction of frictional contact between two elastic bodies. It has been shown that the model is useful for the analysis of the fretting wear in mechanical components. McColl et al. [23] used the Archard model to develop a finite-element method for simulating the fretting wear in aeroengine transmission

components. Hugnell et al. [24] simulated the wear in a cam follower contact using the model and similarly Sawyer [25] presented an analytical solution for the wear prediction in a simple-cam. Moreover, the simple wear Archard model has been used successfully for the prediction of the wear in various mechanical components, as gears [26]-[29] and bearings [30].

1.4 Fretting wear in spline couplings

Spline couplings are mechanical components used to transmit the torque by means of a certain number of engaging teeth. They find application in system of aero-engines, automotive systems and many other industrial sectors.

Spline couplings can experience fretting wear damage becoming a critical factor for the reliability of the mechanical system. It is the relative motion between the teeth of the shaft and hub that causes the spline wear.

The entity of fretting wear in spline couplings depends on different factors as the misalignment between the shaft and hub, not adequate lubrication conditions and a wrong design [31]-[32].

Generally, in working conditions it is very difficult to achieve the perfect alignment between the teeth of shaft and hub. In fact, the angular misalignment can derive from errors in design and manufacturing process, or from the variation in the dynamic operating conditions. It is demonstrated that the angular misalignment is the first cause of fretting wear in spline couplings [31]-[33]. Then, the design process should ever consider the presence of misalignment in order to reduce the bad effects and make a minimum misalignment acceptable.

It is known that the geometry of the spline teeth strongly influences the entity of the fretting wear. The teeth of involute spline couplings can be “straight” or “crowned”. In these two configurations the contact regime is completely different. Many studies focused on the comparison between the two geometries finding that the crowned teeth geometry better allow the angular misalignment, promoting less fretting wear [31], [32], [34]. The distribution of the load on the flanks of the teeth changes dependently from the tooth profile [35]. When spline couplings with straight teeth work in misaligns conditions, the contact establishes only on a portion of the tooth face width and this may cause uneven reacting loads, a complex pressure distribution and a non-uniform load distribution between teeth [36]. For this reason, in some works, the tooth profile modification has been be implemented in order to improve the fretting wear performances [35], [37].

As mentioned above, also the lubrication conditions influence the fretting wear. The lubrication is directly related to the Coefficient of Friction (CoF) establishing between the sliding surfaces [31], [39]. It is demonstrated that lubricant (oil or grease) can reduce the wear more than 60% [32]. Then, the reduction of the CoF becomes a very important goal to achieve for reducing

wear. For this scope, not only oil or grease have been considered, but also surface treatments and coatings can be investigated [31].

Different wear mechanisms as adhesive wear, oxidation wear and abrasive wear can coexist on spline couplings [38]. If lubricated teeth experience an uneven load and then direct contact between the teeth, the local heating leads to adhesion with relative debris formation. The metal particles finding in the lubricated environment induce oxidation wear. Moreover, being the teeth of shaft and hub very close, the trapped particles can produce abrasive wear.

The prediction of fretting wear is a complex issue because of the many variables involved as contact pressure, slip amplitude, wear coefficient, debris distribution and microstructure and environment. This prediction becomes more complicated in case of complex engineering assemblies (as spline couplings) that experience fretting damage. In particular, the complex relationship of the fretting wear with the slip regime and the progressive production of wear debris make difficult the detection of a quantitative model of fretting wear for spline couplings. Many authors based their investigation about wear prediction on spline couplings using the Archard model. In these works, the law is used to implement FEM models of spline couplings by means of it is possible to predict wear in defined circumstances [35]-[42]. In fact, the numerical simulations permit to calculate the slip and contact pressure distribution needed on the Archard law. The numerical approach is commonly coupled with a series of experimental tests on very simple specimen configuration by which the wear coefficient is detected.

The experimental tests in research about wear in spline couplings are very difficult to perform because of the very complex geometry and of the many parameters involving on the phenomenon. Some experimental tests involved only basic configurations [43], [44], but in this case it is difficult to find the correlation between this simplified test and the real fretting behaviour. As a consequence, some authors created dedicated workbench for the investigation on spline wear [45], [46], [47]. An interesting research was conducted by Cuffaro et al. [48]. They developed a test rig capable to allow misalignment between hub and shaft, and, then to simulate the real working conditions.

1.5 References

[1]. Waterhouse, R. B. (1992). Fretting fatigue. International materials reviews, 37(1), 77-98.

[2]. Waterhouse, R. B. (1984). Fretting wear. Wear, 100(1-3), 107-118.

[3]. Uhlig, H. H. (1954). Mechanism of fretting corrosion. Journal of Applied Mechanics-Transactions of the ASME, 21(4), 401-407.

[4]. Hurricks, P. L. (1970). The mechanism of fretting - a review. Wear, 15(6), 389-409.

[5]. Aldham, D., Warburton, J., & Pendlebury, R. E. (1985). The unlubricated fretting wear of mild steel in air. Wear, 106(1-3), 177-201.

[6]. Vingsbo, O., & Söderberg, S. (1988). On fretting maps. Wear, 126(2), 131-147.

[7]. Nishioka, K., & Hirakawa, K. (1969). Fundamental Investigations of Fretting Fatigue: (Part 5, The Effect of Relative Slip Amplitude). Bulletin of JSME, 12(52), 692-697.

[8]. Lewis, R., Slatter, T. Design for reduced wear. ASTM Manual - MNL1-9TH, Chapter 17.

[9]. Querlioz, E., Ville, F., Lenon, H., & Lubrecht, T. (2007). Experimental investigations on the contact fatigue life under starved conditions. Tribology International, 40(10-12), 1619-1626.

[10]. Archard, J. F. (1959). The temperature of rubbing surfaces. Wear, 2(6), 438-455.

[11]. Farrell, R. M., & Eyre, T. S. (1970). The relationship between load and sliding distance in the initiation of mild wear in steels. Wear, 15(5), 359-372.

[12]. Quinn, T. F. J., Baig, A. R., Hogarth, C. A., & Müller, H. (1973). Transitions in the Friction Coefficients, the Wear Rates, and the Compositions of the Wear Debris Produced in the Unlubricated Sliding of Chromium Steels. ASLE TRANSACTIONS, 16(4), 239-244.

[13]. Razavizadeh, K., & Eyre, T. S. (1982). Oxidative wear of aluminium alloys. Wear, 79(3), 325-333.

[14]. Liu, Y., Asthana, R., & Rohatgi, P. (1991). A map for wear mechanisms in aluminium alloys. Journal of materials science, 26(1), 99-102.

[15]. Chen, H., & Alpas, A. T. (2000). Sliding wear map for the magnesium alloy Mg-9Al-0.9 Zn (AZ91). Wear, 246(1-2), 106-116.

[16]. Meng, H. C. (1994). Wear modeling: evaluation and categorization of wear models.

[17]. Archard, J. (1953). Contact and rubbing of flat surfaces. Journal of applied physics, 24(8), 981-988.

[18]. Holm, R. (1946). Electric contacts. Almqvist and Wiksells Boktryckeri.

[19]. Lewis, R. (2007). A modelling technique for predicting compound impact wear. Wear, 262(11-12), 1516-1521.

[20]. Bayer, R. G., Clinton, W. C., Nelson, C. W., & Schumacher, R. A. (1962). Engineering model for wear. Wear, 5(5), 378-391.

[21]. Goryacheva, I. G., Rajeev, P. T., & Farris, T. N. (2001). Wear in partial slip contact. Journal of Tribology, 123(4), 848-856.

[22]. Johansson, L. (1994). Numerical simulation of contact pressure evolution in fretting. Journal of tribology, 116(2), 247-254.

[23]. McColl, I. R., Ding, J., & Leen, S. B. (2004). Finite element simulation and experimental validation of fretting wear. Wear, 256(11-12), 1114-1127.

[24]. Hugnell, A. B. J., Bjoerklund, S., & Andersson, S. (1996). Simulation of the mild wear in a cam-follower contact with follower rotation. Wear, 199(2), 202-210.

[25]. Sawyer, W. G. (2001). Wear predictions for a simple-cam including the coupled evolution of wear and load. Lubr. Eng, 57(9), 31-36.

[26]. Andersson, S., & Eriksson, B. (1990, June). Prediction of the sliding wear of spur gears. In Proceedings of the Fourth Nordic Symposium on Tribology NORDTRIB '90, Hirtshals, Denmark (pp. 10-13).

[27]. Flodin, A., & Andersson, S. (1997). Simulation of mild wear in spur gears. Wear, 207(1-2), 16-23.

[28]. Flodin, A., & Andersson, S. (2000). Simulation of mild wear in helical gears. Wear, 241(2), 123-128.

[29]. Brauer, J., & Andersson, S. (2003). Simulation of wear in gears with flank interference—a mixed FE and analytical approach. Wear, 254(11), 1216-1232.

[30]. Olofsson, U., Andersson, S., & Björklund, S. (2000). Simulation of mild wear in boundary lubricated spherical roller thrust bearings. Wear, 241(2), 180-185.

[31]. Ku, P. M., & Valtierra, M. L. (1975). Spline wear-effects of design and lubrication. Journal of Engineering for Industry, 97(4), 1257-1263.

[32]. Cuffaro, V., Curà, F., & Mura, A. (2014). Experimental investigation about surface damage in straight and crowned misaligned splined couplings. In Key Engineering Materials (Vol. 577, pp. 353-356). Trans Tech Publications.

[33]. Buckingham, E. (1961). How to evaluate the effects of spline misalignments. Machinery, 67, 120-128.

[34]. Medina, S., & Olver, A. V. (2002). Regimes of contact in spline couplings. Journal of tribology, 124(2), 351-357.

[35]. Leen, S. B., Richardson, I. J., McColl, I. R., Williams, E. J., & Hyde, T. R. (2001). Macroscopic fretting variables in a splined coupling under combined torque and axial load. The Journal of Strain Analysis for Engineering Design, 36(5), 481-497.

[36]. Cura, F., Mura, A., & Gravina, M. (2013). Load distribution in spline coupling teeth with parallel offset misalignment. Proceedings of the Institution of Mechanical Engineers, Part C: Journal of Mechanical Engineering Science, 227(10), 2195-2205.

[37]. Ding, J., McColl, I. R., & Leen, S. B. (2007). The application of fretting wear modelling to a spline coupling. Wear, 262(9-10), 1205-1216.

[38]. Xue, X., Wang, S., & Li, B. (2016). Modification methodology of fretting wear in involute spline. Wear, 368, 435-444.

[39]. Ratsimba, C. H. H., McColl, I. R., Williams, E. J., Leen, S. B., & Soh, H. P. (2004). Measurement, analysis and prediction of fretting wear damage in a representative aeroengine spline coupling. Wear, 257(11), 1193-1206.

[40]. Madge, J. J., Leen, S. B., & Shipway, P. H. (2007). The critical role of fretting wear in the analysis of fretting fatigue. Wear, 263(1-6), 542-551.

[41]. Hyde, T. R., Leen, S. B., & McColl, I. R. (2005). A simplified fretting test methodology for complex shaft couplings. Fatigue & Fracture of Engineering Materials & Structures, 28(11), 1047-1067.

[42]. Leen, S. B., McColl, I. R., Ratsimba, C. H. H., & Williams, E. J. (2003). Fatigue life prediction for a barrelled spline coupling under torque overload. Proceedings of the Institution of Mechanical Engineers, Part G: Journal of Aerospace Engineering, 217(3), 123-142.

[43]. Ramesh, R., & Gnanamoorthy, R. (2006). Development of a fretting wear test rig and preliminary studies for understanding the fretting wear properties of steels. Materials & design, 27(2), 141-146.

[44]. McColl, I. R., Ding, J., & Leen, S. B. (2004). Finite element simulation and experimental validation of fretting wear. Wear, 256(11-12), 1114-1127.

[45]. Wavish, P. M., Houghton, D., Ding, J., Leen, S. B., Williams, E. J., & McColl, I. R. (2009). A multiaxial fretting fatigue test for spline coupling contact. Fatigue & Fracture of Engineering Materials & Structures, 32(4), 325-345.

[46]. Leen, S. B., Hyde, T. R., Williams, E. J., Becker, A. A., McColl, I. R., Hyde, T. H., & Taylor, J. W. (2000). Development of a representative test specimen for frictional contact in spline joint couplings. The Journal of Strain Analysis for Engineering Design, 35(6), 521-544.

[47]. Leen, S. B., Hyde, T. H., Ratsimba, C. H., Williams, E. J., & McColl, I. R. (2002). An investigation of the fatigue and fretting performance of a representative aero-engine spline coupling. The Journal of Strain Analysis for Engineering Design, 37(6), 565-583.

[48]. Cuffaro, V., Curà, F., & Mura, A. (2014). Test rig for spline couplings working in misaligned conditions. Journal of Tribology, 136(1), 011104.

2 Contact pressure, sliding and wear volume prediction

2.1 Contact Pressure

The first engineering variable involved in the wear damage of spline couplings is the contact pressure established between two engaging teeth. The value of the contact pressure and the shape of the contact area strongly depend from the local geometry of the two bodies in contact, then from the microgeometry of the teeth.

There are two different geometries used for the teeth of the spline couplings: the straight teeth and the crowned teeth. For the two different configurations, having similar way to work, the contact pressure distribution will be different. In particular, the simple contact between straight teeth is generally modelled as a punch, while for the crowned teeth the contact conditions are more complicated and the modelling require the use of the hertzian theory [1].

In this chapter, a numerical model of crowned spline couplings, developed to study the contact pressure phenomenon, will be presented. The FEM model have been validated using the Hertzian theory.

On the basis of the numerical model, the goal of this paragraph will be the evaluation of the microgeometry parameters influencing directly the contact pressure, in order to better understand their role during the design phase.

2.1.1 FEM model

As mentioned above, a set of FEM models of crowned spline couplings have been carried out in order to evaluate the contact pressure between the teeth and to identify the most important microgeometry parameters influencing it. The numerical simulations have been built by means of Abaqus Software.

The spline coupling geometry has been chosen according to DIN 5480-1 [2] (modulus m=3, reference diameter dB=50 mm). The basic rack profile is shown

in Figure 2.1. All representative parameters of the spline coupling in its basis configuration are reported in Table 2.1.

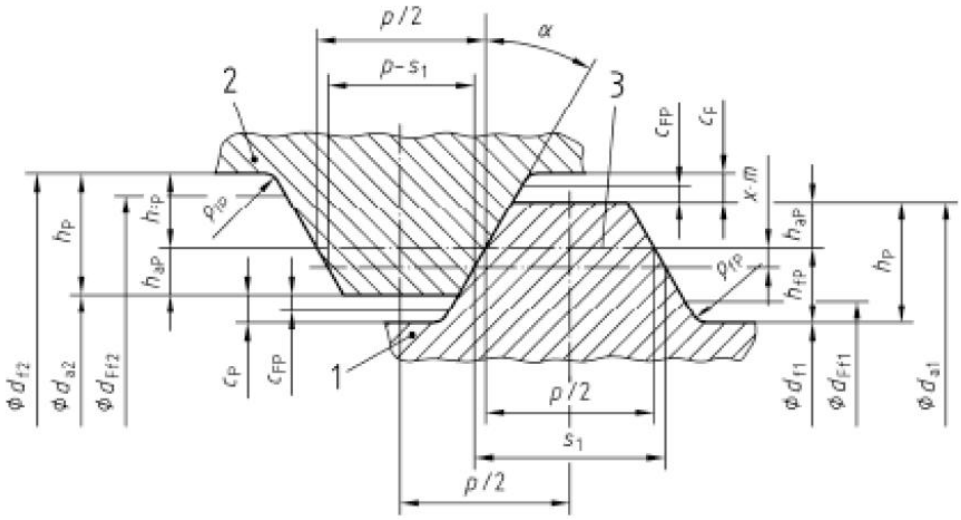

Figure 2.1. Shaft and hub teeth profile main dimensions (DIN 5480-1).

Number of teeth	Addendum modification coefficient	Reference circle diameter	Base diameter	Tip circle diameter	Root circle diameter
Z	$x_1 = -x_2$	D	d_b	d_{a2}	d_{f2}
15	0.28	45	38.97	44	50

Root form circle	Tip circle diameter	Root circle diameter	Base form circle diameter	Nominal tooth thickness	Nominal space with
d_{Ff2min}	d_{a1}	d_{f1}	d_{Ff1max}	s_1	e_2
49.47	49.40	43.40	43.93	5.69	5.69

Table 2.1. Spline couplings parameters; 1: shaft, 2: hub. Dimensions in mm.

For the FEM model first-order tetrahedral solid elements have been used throughout. The mesh size in the contact area is very fine (about 0.2 mm) to better fit the geometry and to decrease the error. The material of both shaft and hub has been defined using Young modulus E=210 GPa and Poisson coefficient ν=0.3. In order to define the contact behaviour between the teeth, contact surfaces in each tooth have been created (as it can be seen in Figure 2.2). A surface interaction named “contact pair” has been chosen; a type “surface-to-surface” discretization has been chosen instead of the “node-to-surface”: <<the “surface-to-surface” enforces contact conditions in an average sense over regions nearby slave nodes rather than only at individual slave nodes>> [3]. The contact tracking approach is of the type” finite-sliding tracking” that allows for

arbitrary separation, sliding, and rotation of the surfaces. The coefficient of friction between the surfaces in contact has been set equal to 0.11, which corresponds to the average value typically found for the material considered.

Torque about shaft axis has been applied on the extremity of the shaft, while displacements related to all directions have been blocked on the opposite extremity of the hub.

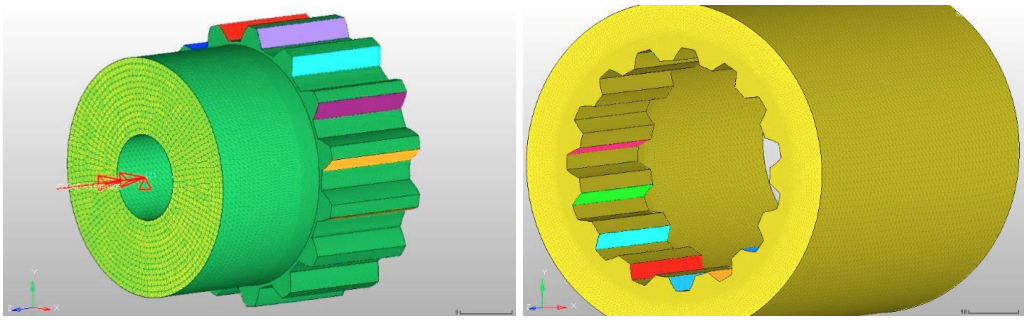

Figure 2.2: FEM model of the spline coupling: shaft (left) and hub (right).

Abaqus gives a series of results related to the contact analysis such as contact pressure (command CPRESS) and frictional shear stress (CSHEAR) or relative tangential motions (CSLIP).

Figure 2.3 shows an example of numerical results in terms of contact pressure distribution (CPRESS) on the shaft (left) and on the hub (right). Also, the shape of the contact area is emphasized in this figure.

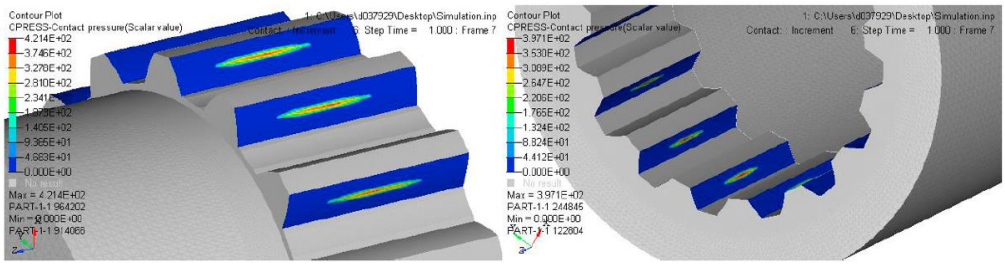

Figure 2.3. Example of numerical results: contact pressure distribution on the shaft (left) and on the hub (right).

The value of the contact pressure, the shape of the elliptical contact area (represented by the ratio between the half-axis) and its position along the length width and with respect to the involute profile are the most important parameters to consider. The position of the contact area with respect to the length width can give informations about the presence of misalignment or not: if the footprint is not centred with respect to the centre line of the tooth, there would be misalignment.

2.1.2 Validation of FE results using the hertzian theory

As mentioned above, for the analytical calculation of the contact pressure the theoretical models considered is the well-known hertzian theory [4]. The pressure values calculated from the hertzian theory consist in maximum and mean pressure values and the corresponding contact area entity.

Considering the contact between the teeth, the contact area is an ellipse of semi-major axis *a* and semi-minor axis *b* calculated as follow:

$$a = \mu\, q$$
$$b = \nu\, q$$

being:

- μ and ν coefficients functions of an auxiliary angle $\cos\tau$ defined as:

$$\cos\tau = \frac{(\rho_{1max} - \rho_{1min}) - (\rho_{2max} - \rho_{2\min})}{\sum\rho}$$

  and $\sum\rho = \rho_{1max} + \rho_{1min} + \rho_{2max} + \rho_{2min}$, in which ρ_{1max}, ρ_{1min}, ρ_{2max} and ρ_{2min} are the maximum and minimum curvatures of the two bodies;

- q a parameter depending from the contact force F, and the characteristics of the material of the two bodies, calculated as:

$$q = \sqrt[3]{\frac{3}{8} F \frac{\theta_1 + \theta_2}{\sum\rho}}$$

  where $\theta_i = 4\frac{m_i^2 - 1}{m_i^2 E_i}$, in which m_i is the Poisson modulus and E_i is the Young modulus of the -ith body.

Following the results of the theory, the mean contact pressure is:

$$p_{mean} = \frac{F}{\pi\, a\, b}$$

And the maximum contact pressure is:

$$p_{mean} = 1.5\, p_{mean}$$

As can be seen, to calculate the hertzian contact pressure between the engaging teeth, the equivalent curvatures of the two bodies in contact must be obtained. Due to the tooth pair geometry the contact problem may be approximated as an elliptic contact problem. In this case 4 curvature radii must be obtained (two for the shaft tooth and two for the hub). The problem can be divided into two planes: one parallel to the tooth with and the other parallel to

the tooth profile. In this way 4 radius of curvature have been identified (see Figure 2.4):

- R1x: radius of curvature of the shaft along x plane (crowning radius);
- R1y: radius of curvature of the shaft along y plane (involute radius);
- R2x: radius of curvature of the hub along x plane (crowning radius);
- R2y: radius of curvature of the hub along y plane (involute radius).

In particular, for as concerns the shaft, the crowning radius R1x is related to the minimum curvature ρ_{1min} and the involute radius R1y is related to the maximum one ρ_{1max}. For as concerns the hub no crowning radius has been considered (maximum curvature ρ_{2max} is zero) and the involute radius corresponds to minimum curvature ρ_{2min}.

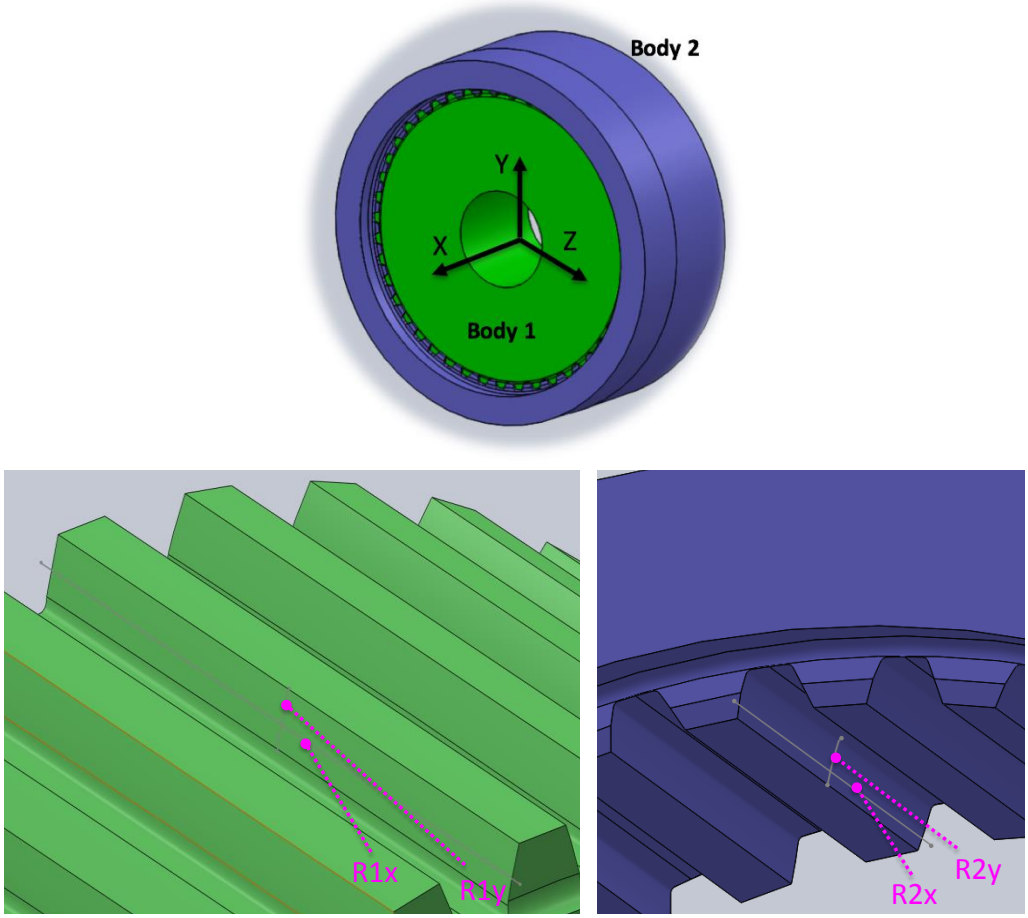

Figure 2.4: Curvature radii of the shaft (left) and hub (right).

The contact force, depending on the applied torque, has been calculated as the equivalent force applied at the average contact diameter (Figure 2.5). The force is inclined by the pressure angle. This is an approximation as the pressure angle of 20° should be only at the pitch diameter, but is acceptable as an error

on the real pressure angle of 2° brings to a difference in the force calculation of 1.3%.

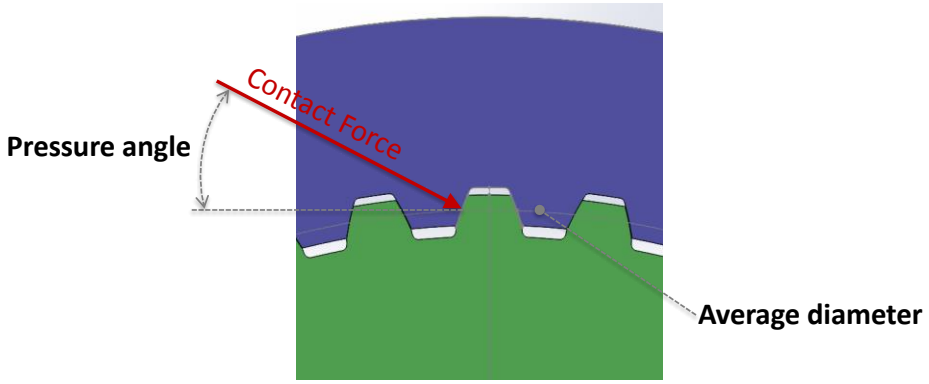

Figure 2.5: Contact force calculation.

Table 2.2 shows the percentage of difference on the results of Hertzian theory and numerical model in terms of maximum contact pressure, mean contact pressure and contact area.

Parameters	%Diff.
Maximum Contact Pressure [MPa]	4.9
Mean Contact Pressure [MPa]	10.9
Contact area [mm^2]	8.9

Table 2.2. Results comparison between Hertz theory and FEM.

The value of the maximum contact pressure calculated by FEM is higher respect to the Hertzian model by only 4.9%, while the mean contact pressure value is 10.9% lower than the theoretical model. The related difference on the value of the contact area is 8.9%.

On the basis of the above results, the difference on the results between theoretical and the FEM model seems acceptable.

The main difference between Hertz's model and FE model is that in the first one the contact geometry is approximated by ellipses while in the FE models the geometry is the actual one. Then, the difference between FE and Hertz results could be related to the above quoted approximation in the geometry. Moreover, it is important to remember that the Hertz theory is based on the hypothesis of perfect elasticity of the material and absence of friction force.

2.1.3 Microgeometry parameters influencing the contact pressure

The sensitivity analysis for the microgeometry parameters involves some micro corrections of the tooth geometry, related firstly to the crowning radius and then to the involute profile. In Figure 2.6 the scheme of the involute correction is presented. Only the modification of the shaft profile has been considered: the red profile represents the new shaft profile, the contact point (on the average diameter) between the teeth remains the same.

For the different numerical models developed to investigate the problem, all calculations have been made considering different values of applied torque, maximum and minimum curvatures of the shaft. In particular, two torque levels have been applied, 500 Nm and 700 Nm; four values of ρ_{1max} have been used, 1/11.3, 1/10.9, 1/10.5 and 11/10.7 mm^{-1}; three values of ρ_{1min} have been chosen: 1/5000, 1/4000 and 1/3000 mm^{-1}; ρ_{2min} has been set as -1/14.05 mm^{-1} for all cases. For each possible combination of these three parameters, maximum contact pressure p_{max}, mean contact pressure p_{mean}, contact area and ratio a/b between half-axis of the contact ellipse (respectively maximum and minimum) have been calculated. In Table 2.3 the microgeometry parameters of the 6 models developed are presented.

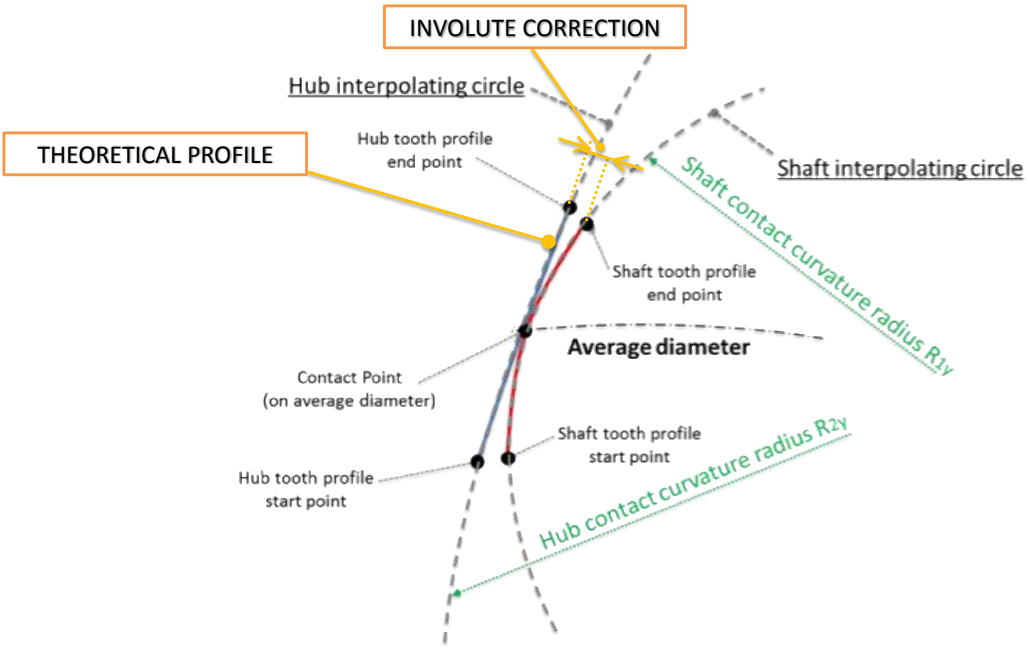

Figure 2.6: Involute correction scheme.

Model	Torque [Nm]	ρ_{1max}[mm^{-1}]	ρ_{1min}[mm^{-1}]	ρ_{2max} [mm^{-1}]	ρ_{2min} [mm^{-1}]
m1	500	1/11.3	1/3000	0	-1/14.051
m2	500	1/10.5	1/3000	0	-1/14.051
m3	500	1/10.7	1/3000	0	-1/14.051
m4	700	1/10.9	1/3000	0	-1/14.051
m5	700	1/10.7	1/4000	0	-1/14.051
m6	700	1/10.9	1/4000	0	-1/14.051

Table 2.3. FEM models parameters.

Figure 2.7 shows an example of FEM results in terms of contact pressure distribution on the shaft for three different model: m1, m2 and m3. The shape of the contact area, emphasized in this figure, is elliptical for every model. As expected, the main difference is related to the value of the max contact pressure and the position of the foot print respect to the tooth profile, depending on the value of the involute radius applied.

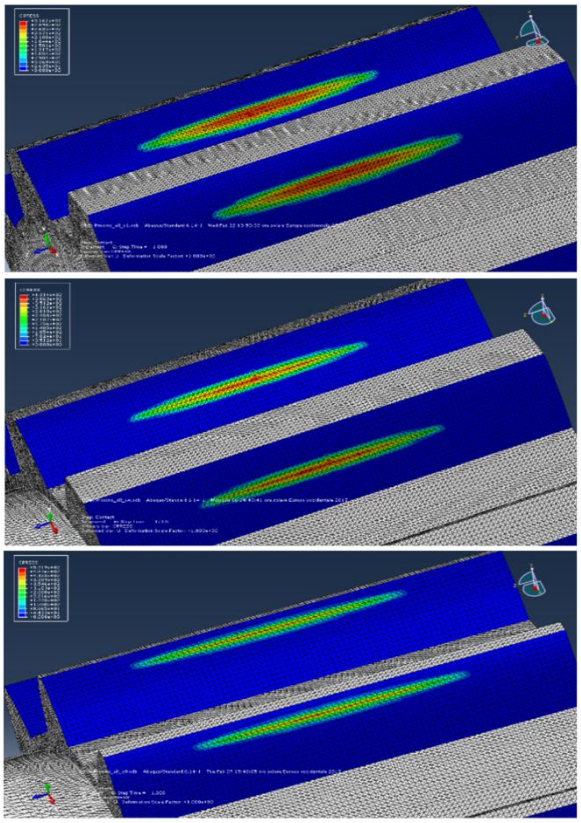

Figure 2.7. Example of FEM results: contact pressure distribution of the model m1 (up), m2 (centre) and m3 (down).

Figure 2.8, Figure 2.9 and Figure 2.10 show respectively the trend of both maximum and mean contact pressures and of the contact area by varying the microgeometries of the shaft, obtained by analytical and FE calculations. In

particular, maximum and mean contact pressure and contact area are represented as a function of the maximum curvature ρ_{1max} (related to the involute radius) and the crowned radius, or better the minimum curvature ρ_{1min}, acts as a curve parameter. It may be noted that, as expected, the entity of microgeometries strongly influences the contact parameters. In particular, the variation of the involute curvature radius makes possible to tune the actual value of the maximum pressure together with the contact area. As expected, all curves are shifted by the increase of the torque level in the direction of a corresponding damage increasing; this represents a local phenomenon.

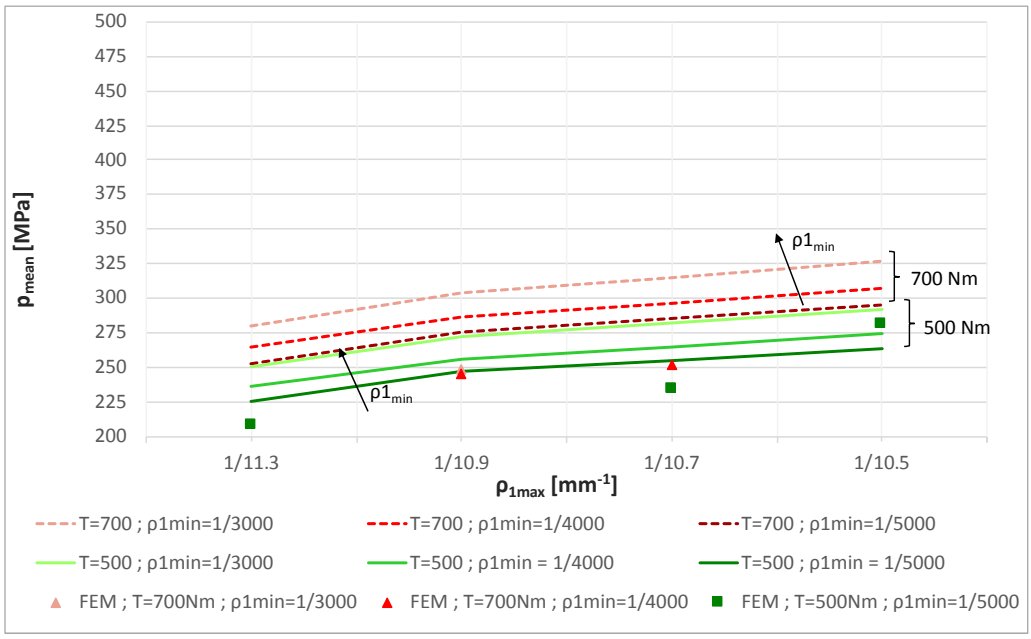

Figure 2.8: Mean contact pressure trends: analytical and numerical results.

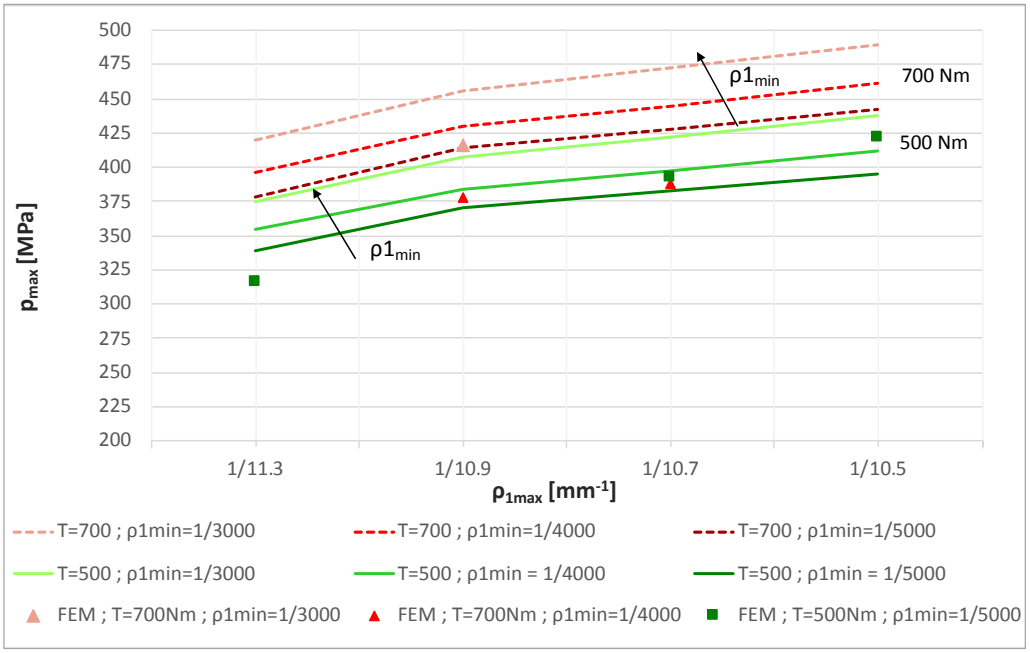

Figure 2.9: Maximum contact pressure trends: analytical and numerical results.

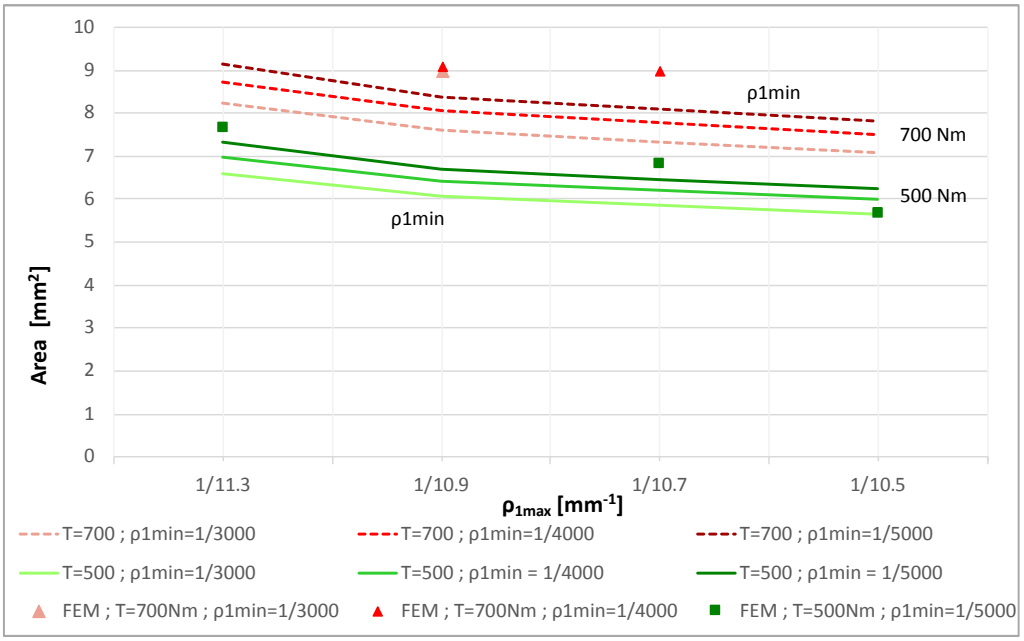

Figure 2.10: Contact area trends: analytical and numerical results.

2.2 Sliding evaluation

On the basis of the Archard law, in addition to the contact pressure, the other very important parameter influencing the fretting wear is the “sliding”. In fact, as explained in the previous paragraph, it is the relative motion between teeth in contact that may usually create a surface damage and the corresponding progressive loss of material.

In spline couplings, the total relative sliding between engaging teeth is due to two contributes:

- kinematic movement due to angular misalignment;
- tooth deflection due to the tooth deflection

The kinematic movement caused by angular misalignment can be calculated on the basis of kinematic considerations, while the sliding due to the tooth deflection can be evaluated using the developed numerical models. The total sliding will be the resultant of these two displacements.

2.2.1 Sliding due to the misalignment

The kinematic sliding is due to the kinematic relative movements of engaging teeth during the shaft rotation when shaft and hub work in misalignment conditions. When the spline coupling is aligned, the load distribution among engaging teeth is uniform, as investigated by means of both numerical and theoretical approaches, by some authors [5], [6], [7]. In this case (aligned spline), no spurious loads are generated. In the other hand angular misalignment causes a modification in teeth loading, bringing to a non-uniform load distribution among engaging teeth [8],[9],[10]. Curà and Mura [11] in 2017 analysed the reacting loads caused by the presence of misalignment in spline couplings.

Straight teeth in splined couplings should work only in aligned condition, while crowned teeth may allow a little angular misalignment between hub and shaft. Anyway, it happens that also straight teeth splined couplings may work in misaligned conditions. In both cases the misalignment is allowed only by the clearance between teeth.

In misalignment conditions (angle α not equal to zero) the contact point, that in aligned conditions belong to a vertical line through the middle point of the face width, moves of a distance "b" respect to the middle line (see Figure 2.11) and this causes the sliding during the revolutions.

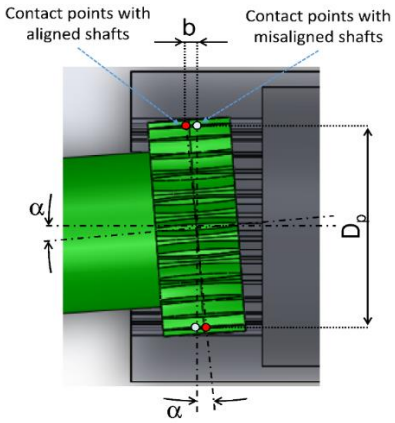

Figure 2.11: Contact point between the teeth in case of misalignment.

Following these considerations, the sliding due to the misalignment can be evaluated on the basis of kinematic formula. Considering the scheme of Figure 2.12, during a revolution the relative displacement of the contact point A of the shaft can be divided in two components: the first one along the x axis (length width) and the second one along the y axis (involute profile), calculated as:

$$X_a = r_m \sin(\alpha \sin(\omega_m t))$$

$$Y_a = r_m - r_m \sin \cos(\alpha \sin(\omega_m t))$$

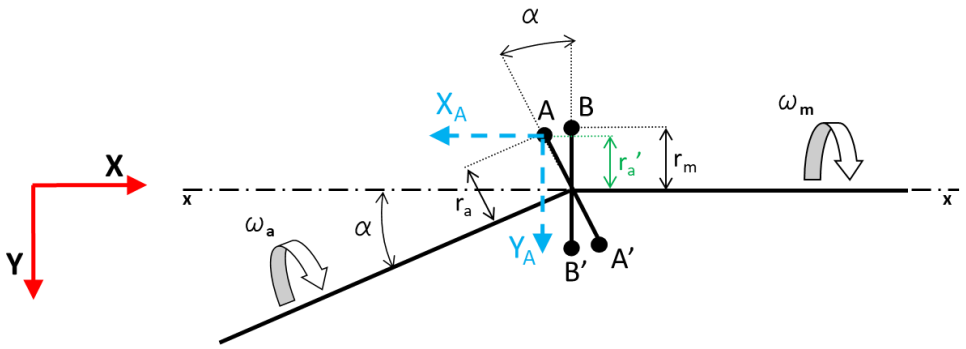

Figure 2.12. Scheme for understanding the components of the contact point displacements.

The sliding of the point calculated at average radius r_m depends on the rotation angle $\omega_m t$ and it is characterized by an harmonic trend. In Figure 2.13 an example of displacements trend during the revolution is reported. As can be seen, the total relative displacement of the point in one cycle will be two times the maximum displacement (the pick value).

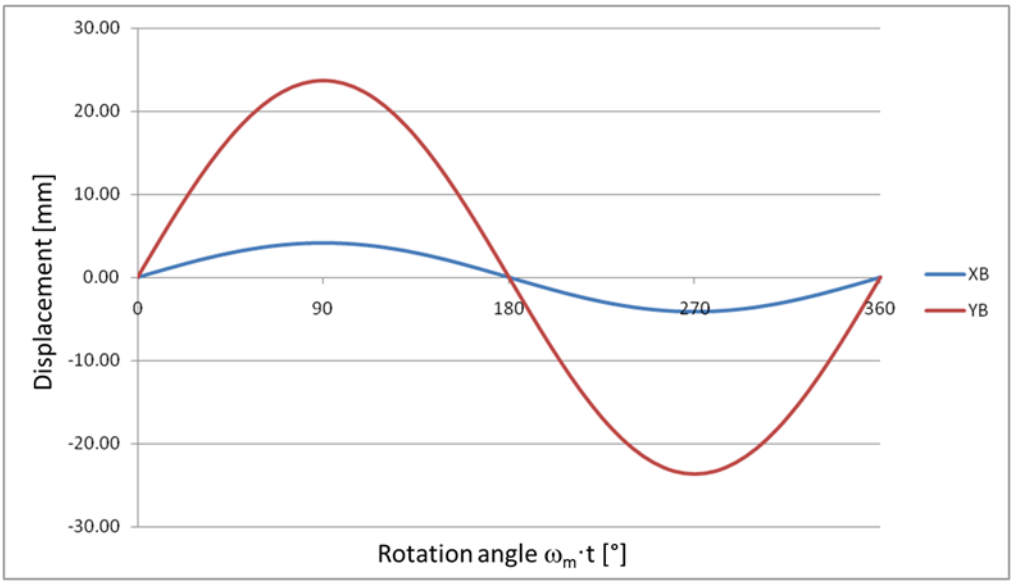

Figure 2.13. Example of relative displacement trend of the contact point during the revolution.

In order to better understand how the contact distribution change in misalignment case, the numerical model has been modified including a misalignment angle between shaft and hub equal to 0.654 mrad. The position of the contact area along the length width varies in harmonic way as the contact point does (Figure 2.14). Moreover, the Figure 2.14 also highlight the possibility to incur in mesh dependency problems when very complex non-linear phenomena are simulated. In this case, the contact pressure distribution shows a discontinuity (a red spot on the middle of the contact area and a distortion from the elliptical shape); that is related to the shape of the mesh that changes exactly in that points (the triangle orientation changes, as they are mirrored). For this reason a new FE model have been developed by changing the mesh of the teeth surface in order to eliminate the discontinuity.

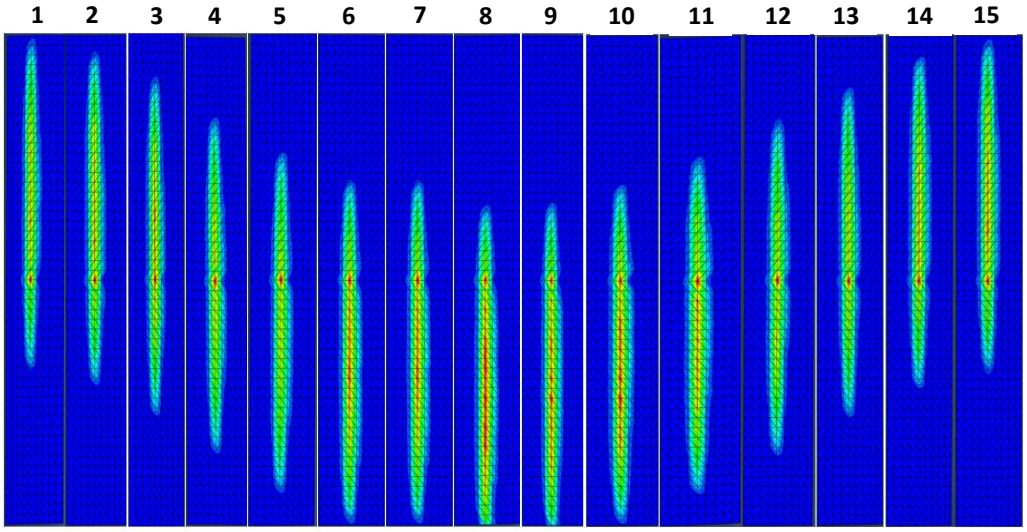

Figure 2.14. Contact pressure distribution on the numerical model in misalignment case.

2.2.2 Sliding due to the tooth deflection

The second sliding type is due to the variable torque: given a load the tooth deflects (see Figure 2.15), if the load is not constant during the spline coupling working, a relative sliding is generated on engaging teeth surfaces. It is easy to understand that the tooth deflection is directly related to the tooth stiffness.

About this phenomenon a recent research has been carried out by Guo and al. [12] in a paper related to wind turbine gearboxes leading to understanding the behaviour of spline connections and providing recommendations to improve design standards.

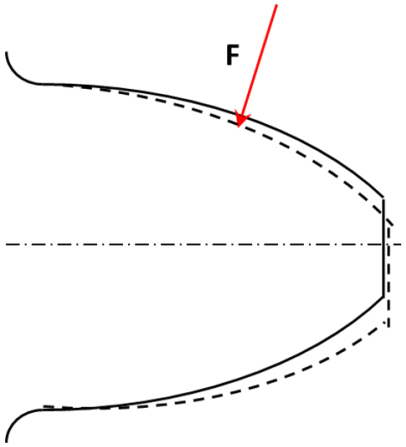

Figure 2.15. Deflection of the teeth when a load (F) is applied.

The evaluation of the sliding due to the load change can be made using the FEM simulations. By means the command "CSLIP", Abaqus provides the results in terms of relative tangential displacements on the x axis (CSLIP1) and y axis (CSLIP2). Figure 2.16 represents an example of relative tangent displacement values, involved in torque application in aligned conditions.

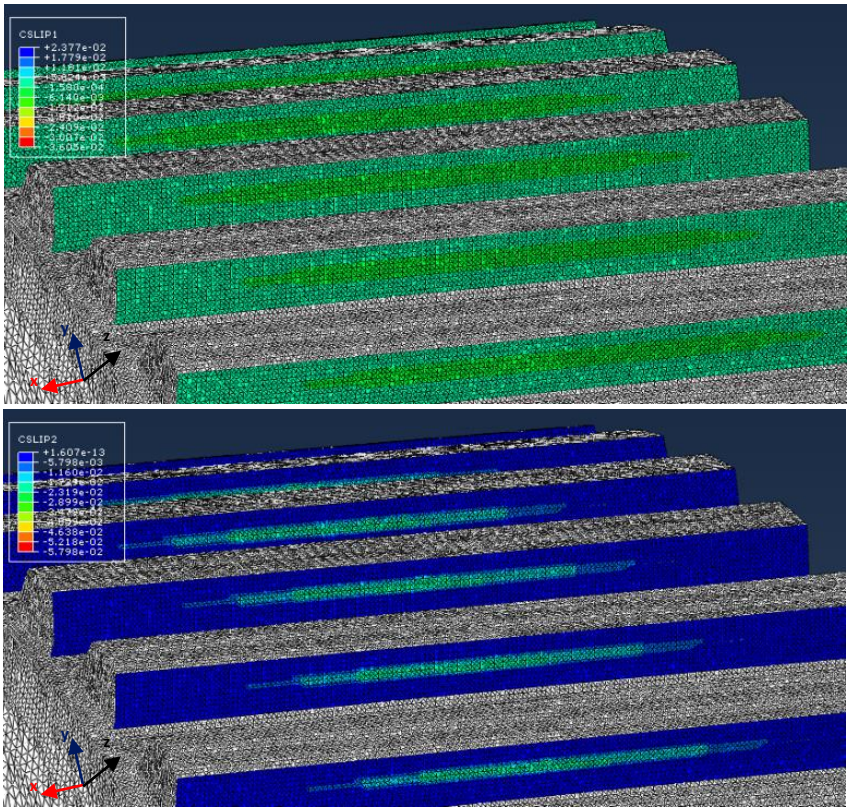

Figure 2.16. Example of relative tangential displacement results: CSLIP1 results (up) and CSLIP2 results (down). Aligned case.

Despite the absence of misalignment, the results reports the presence of sliding in both x axis and y axis. This confirms that there is another source of sliding attributable to the teeth deflection when the torque varies from zero to

the maximum value. The distribution of the sliding reflects the contact pressure distribution characterized by an elliptical shape.

As expected, the addition of the misalignment to the numerical model causes the rise of the relative tangential displacements for both directions (see Figure 2.17) and the displacement of the maximum values outside the centre of the teeth length.

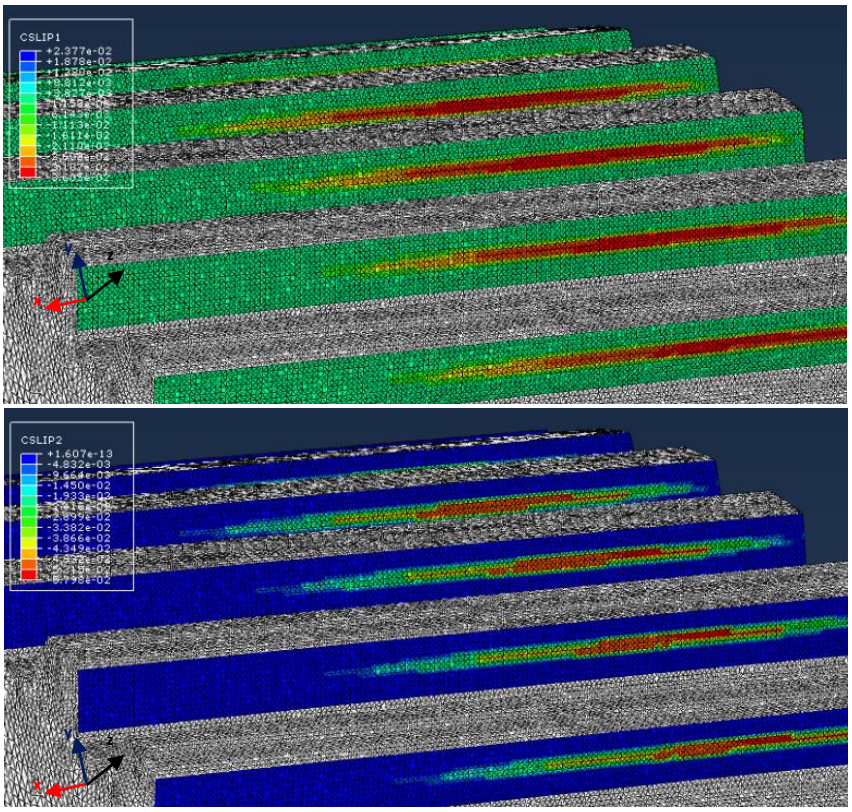

Figure 2.17. Example of relative tangential displacement results: CSLIP1 results (up) and CSLIP2 results (down). Misaligned case.

2.2.3 Influence of tooth flexibility on the sliding

As mentioned above, the tooth stiffness directly influences the entity of the sliding when the torque is applied on the component. In order to study this effect and understand how the stiffness impacts on the sliding, a series of numerical model have been developed. The FEM model used are the same presented in the previous paragraph and reported in Table 2.3. Every model is characterized by a different teeth stiffness obtained by changing progressively the teeth thickness: about 5% less in each model. In Figure 2.18 an example of results is reported. As can be seen the progressive reduction of the teeth thickness and, then, of the teeth thickness leads to a different sliding distribution and values.

In Table 2.4 the results in terms of sliding values for the FEM model carried out are presented. In every case, the sliding along x axis (corresponding to the

length width direction) are one order of magnitude higher than the sliding along y axis (corresponding to the teeth profile direction). As expected, the increasing on the torque applied (passing from 500 Nm to 700 Nm) causes the rising of the sliding magnitude.

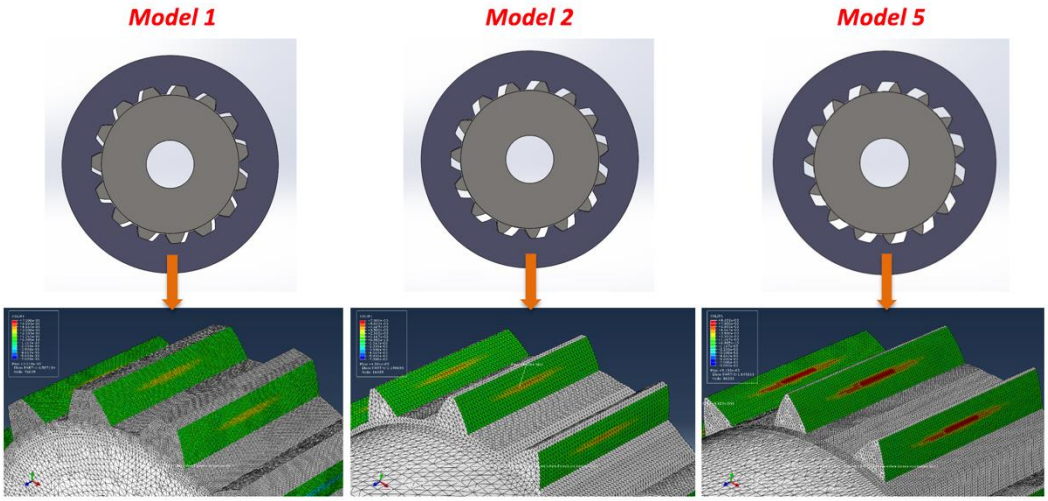

Figure 2.18. Example of sliding distribution for different numerical models.

Model	Torque [Nm]	ρ_{1max} [mm^{-1}]	ρ_{1min} [mm^{-1}]	Slidings x axis [mm]	Sliddings y axis [mm]	Slidings magnitude [mm]
m1	500	1/11.3	1/3000	0.00321	-0.00067	0.00328
m2	500	1/10.5	1/3000	0.00660	-0.00037	0.00661
m3	500	1/10.7	1/3000	0.00391	-0.00035	0.00393
m4	700	1/10.9	1/3000	0.00907	-0.00048	0.00908
m5	700	1/10.7	1/4000	0.00901	-0.00048	0.00902
m6	700	1/10.9	1/4000	0.00886	-0.00051	0.00887

Table 2.4. FEM results: values of sliding.

2.3 Wear volume calculation on damaged spline couplings

Investigating the literature, compared with the development of qualitative understanding of the fretting wear, its quantitative assessment is less well advanced. In this paragraph a method for the evaluation of the wear volume in a damaged spline coupling is presented. To estimate the quantity of material removed during the working of a spline coupling from the profile of the teeth, a mathematical model has been developed.

For this purpose, a series of spline couplings tested on a dedicated test rig have been used. In perfect accordance to that discussed on the previous

paragraphs, analysing the wear surface of the teeth the footprint can be considered to have an elliptical shape (Figure 2.19).

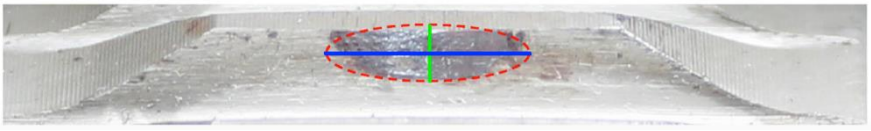

Figure 2.19. Enlargement of the wear scar: the track can be associated to an elliptical shape; in green and in blue we notice respectively the minor and the major axis of the ellipse.

To evaluate the wear extent of the teeth a two-dimensional profilometer (PGS200 Profilometer by SM Instruments) have been used (Figure 2.20).

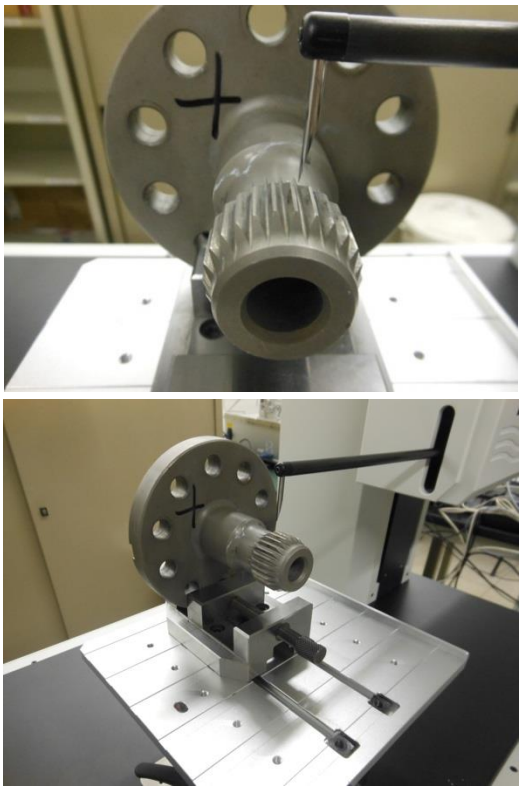

Figure 2.20. Spline couplings fixed to the profilometer ready to be analysed.

By taking the elliptical assumption, during the measure the 4-axis positioner of the instrument have been toned in order to move the tip exactly along the minor axis of the hypothetical ellipse (see green line on the Figure 2.20). Using an unworn surface as a reference surface, the Software of the profilometer prints a curve expressing the amount of offset at each coordinate between the nominal profile and the worn one (Figure 2.21).

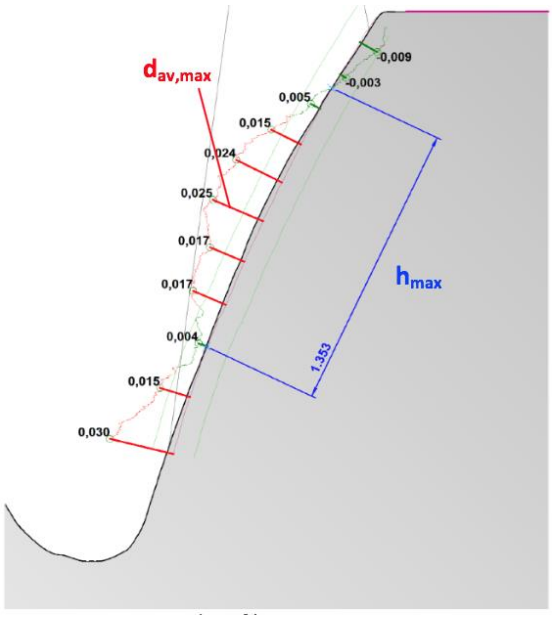

Figure 2.21. Example of profile offset measure using the 2D profilometer.

As can be seen from the Figure 2.21, the distance h_{max} correspond to the minor axis of the ellipse and the maximum depth of the wear scar is $d_{av,max}$.

Moving into 3D environment, the main assumption on the basis of the method is: the wear volume can be approximated as a semi-ellipsoid volume (Figure 2.22).

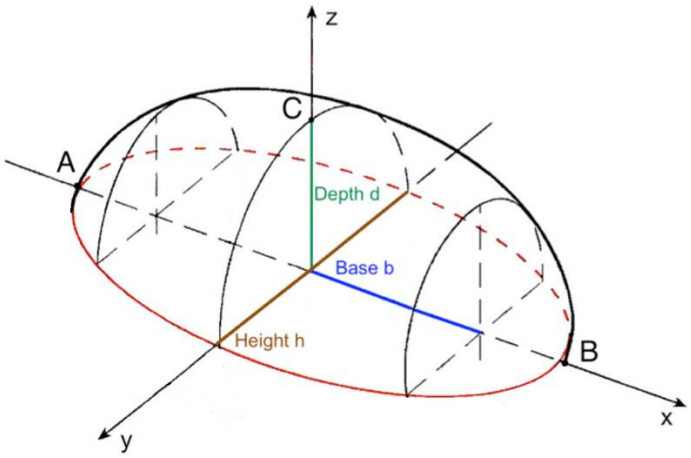

Figure 2.22. Semi-ellipsoid with reported the sizes needed for the calculations.

To calculate such volume the semi-ellipsoid can be discretized into a set of elementary parallelepipeds, characterized by length h_i, width p and height d_i.

Thus, the following hypothesis have been used:

1. the depth of the wear scar d_i through x varies according to a circumference function passing through 3 points: the extremities of the

footprint and the point distant $d_{av,max}$ from its centre; thus, $d\left(x = \frac{c}{2}\right) = 0$ and $d(x = 0) = d_{av,max}$, (

2. Figure 2.23). The footprint length "c" of the wear scar is detected using a calliper;

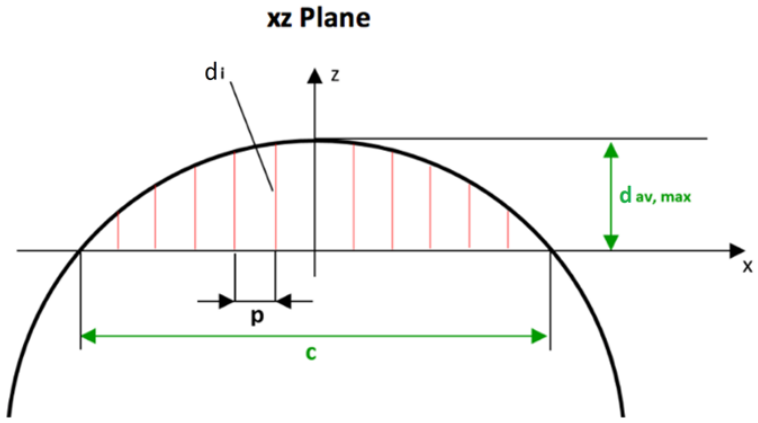

Figure 2.23. xz plane - circumference discretization.

3. assuming that the footprint has elliptical shape, the value of the lengths h_i can be calculated by means an elliptical equation (xy-plane), (Figure 2.24).

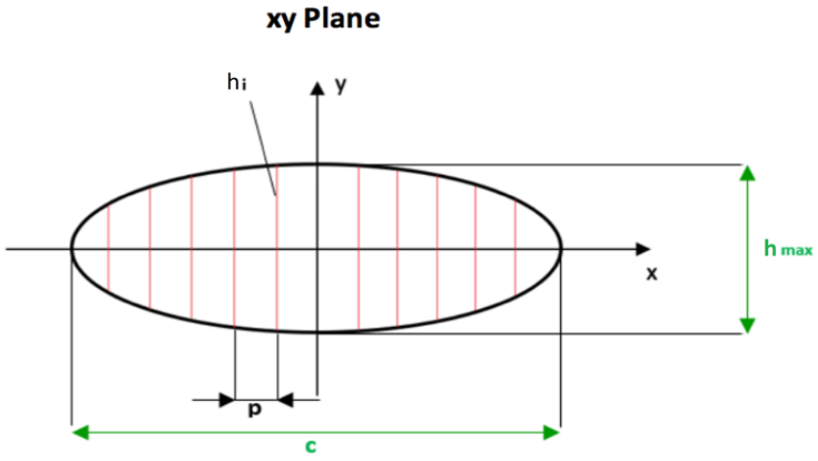

Figure 2.24. xy plane - ellipse discretization.

Table 2.5 resumes the circumference equation and ellipse equation used for the calculations.

Circumference equation $\boldsymbol{x^2 + z^2 + \alpha x + \beta z + \gamma = 0}$	$\alpha = 0$
	$\beta = \frac{\frac{c^2}{2}}{d_{av,max}} - d_{av,max}$
	$\gamma = -(\frac{c}{2})^2$
Ellipse equation $\frac{\boldsymbol{x^2}}{\boldsymbol{a}} + \frac{\boldsymbol{y^2}}{\boldsymbol{b}}$	$a = \frac{c}{2}$
	$b = \frac{c}{2}$

Table 2.5. Circumference equation, ellipse equation and related parameters.

As result of the discrete calculations, the wear volume is:

$$V_{tot} = V_{N+0.5} + 2\left(\sum_{i}^{N} V_i\right)$$

where: $V_{N+0.5} = d_{av,max}\ h_{max}\ p$ is the volume of the parallelepiped lying at the centre, $V_i = d_i\ h_i\ p$ is the volume of the i-th parallelepiped, $p = (c\ /\ 2)/N$ is the step and N the total number of divisions.

Knowing the value of the wear volume V_{tot}, the total sliding amplitude S and the applied load F, the wear coefficient is:

$$k = \frac{V_{tot}}{S\ F}$$

2.3.1 Considerations about the method

The mathematical model for the prediction of the wear volume descripted above presents some limitations. Different experimental texts conducted using a dedicated test rig (for more information see Chapter 3) have demonstrated that the wear damage can be not uniform among the teeth. As an example, in Figure 2.25 some optical microscope images of damaged teeth are shown. The spline couplings (having same dimensions of the model presented in Table 2.1) have been tested with the following conditions: 4' of misalignment, torque equal to 700 Nm, speed 1500 rpm and number of cycle equal to 6 million. The different wear damage result in a different amount of wear volume calculated for each tooth. As a consequence, different values of wear coefficient will be calculated. In this case, an average wear coefficient could be considered.

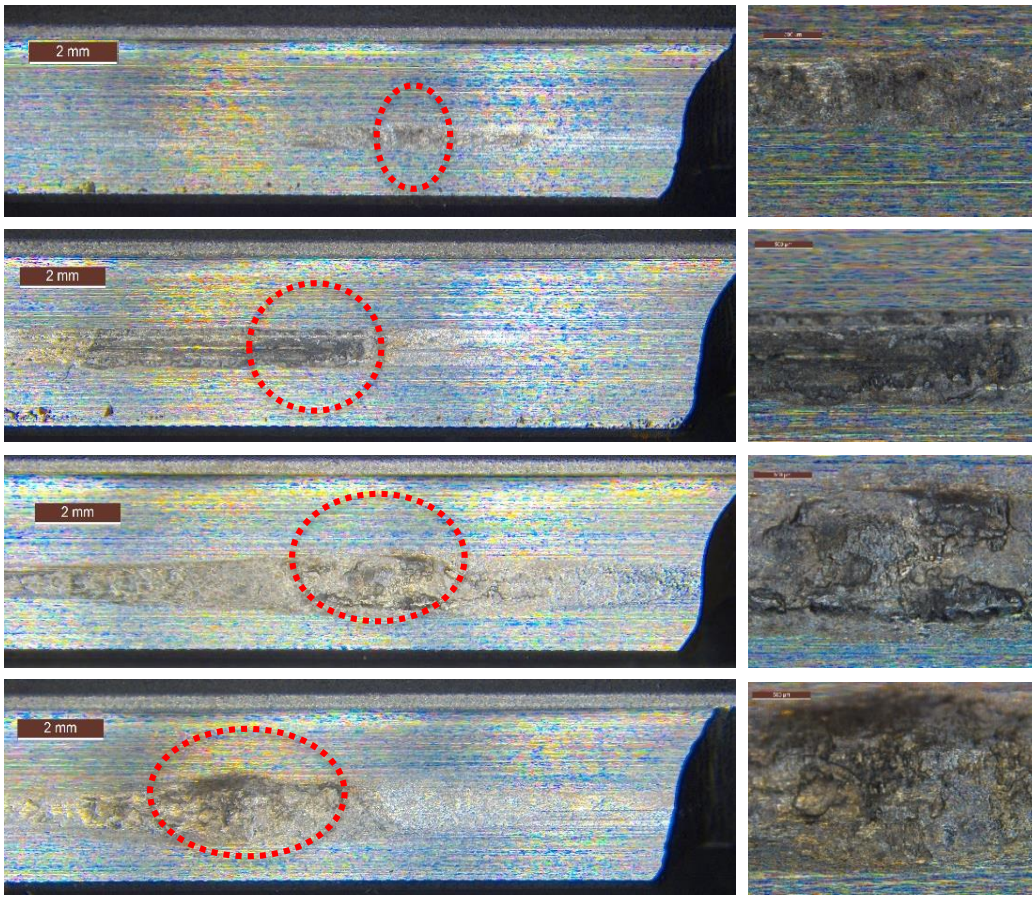

Figure 2.25. Optical Microscope images of damaged teeth after experimental test. (Magnifications at 50x).

As a further limitation of the mathematical model, it is important to consider the different wear mechanisms that can afflict the spline coupling. The method works when the material is removed from the surface of the tooth scanned by the profilometer, then when the tooth surface presents a furrow as a consequence of the wear. This situation emerges when only abrasive wear is present or in case of adhesive wear that causes the removal of material from the surface analysed. There are in fact some cases in which material is deposited on the surface of the tooth. As an example, see Figure 2.26 that shows optical microscope image and profilometer scanning of a damaged tooth. In this case, the profilometer scanning shows particles of material deposited on the tooth surface and the teeth surface appear not uniformly damaged. The explanation of this phenomenon could be related to adhesive wear occurring between shaft and hub: material particles detach from the hub (which is the softest material) welding on the shaft teeth surface.

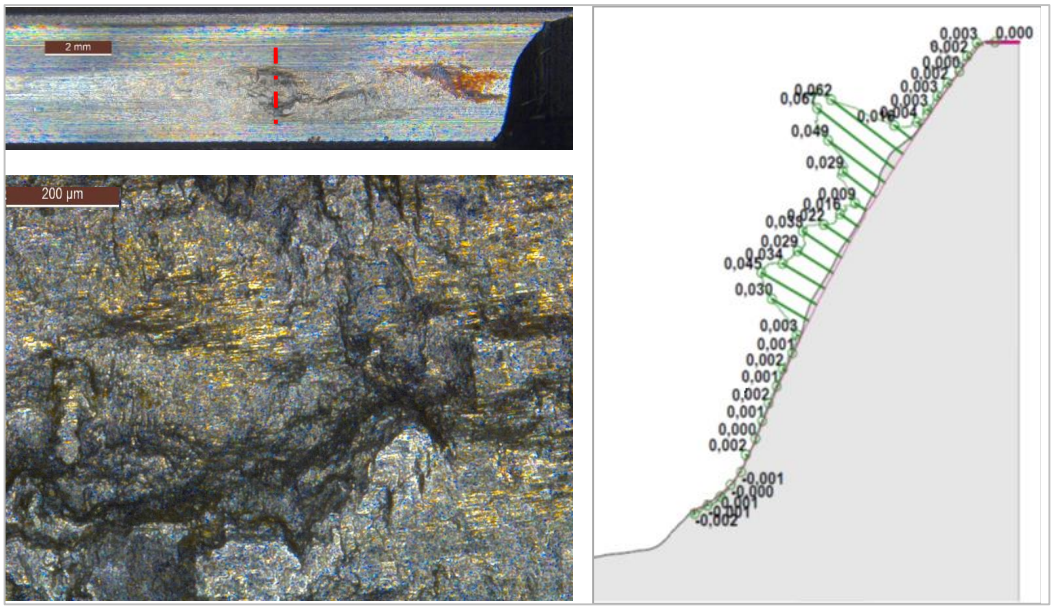

Figure 2.26. Optical Microscope images and profilometer scanning of a damaged spline coupling tooth.

2.4 Wear volume prediction in spline couplings using a tribometer

Goal of this paragraph is the prediction of the wear volume using a pin-on-disk tribometer. The idea on the basis of the method is to develop an experimental procedure able to predict the wear volume of a spline couplings working in certain conditions.

Starting from the Archard law, it is fundamental to define the "equivalent" parameters" to set on the tribometer to perform the experimental tests. In fact, defined the working conditions of the spline coupling for which the wear volume have to be predicted, it is necessary to know the normal load F to apply, the total travelled distance D and the sliding velocity v. It also fundamental to use pin and disc of the same materials of the teeth in contact on the spline couplings.

The normal load F is calculated starting from the value of maximum contact pressure established between the teeth and inserting it on the Hertzian model. For the calculation of the maximum contact pressure a FEM model similar to that presented above can be used (paragraph 1.1.1). Obviously, it is important to set the numerical model with the parameter of the spline couplings examined (geometry and working conditions). From the theory of Hertz, in case of a contact between sphere and plane, the maximum contact pressure is:

$$p_{max} = 0.578 \sqrt[3]{\frac{F\rho^2}{E^{*2}}}$$

Where ρ is the curvature of the pin sphere; $E^* = \left(\frac{1-\nu_1^2}{E_1}\right) + \left(\frac{1-\nu_2^2}{E_2}\right)$ with ν_1, E_1, ν_2 and E_2 Poisson modulus and Young modulus of the two materials in contact. Then, knowing all the above parameters, the load F to set on the tribometer is:

$$F = \frac{p_{max}^3 \, E^{*2}}{0.578^3 \, \rho^2}$$

The total travelled distance D to set on the pin-on-disk apparatus is depending on the sliding per each cycle S that affect the spline coupling and on the total number of cycles performed. The calculation of the sliding S follows the procedure discussed above (paragraph 1.2) based on the evaluation of the two components: the first one related to the misalignment and the second one related to the flexibility of the teeth. The total travelled distance will be equal to:

$$D = S \cdot cycles$$

The sliding velocity v at which the pin-on-disk test have to be performed is calculated as the product between the sliding per each cycle S and the rotational speed of the spline coupling n (in cycle on time):

$$v = S \cdot n$$

At the end of the pin-on-disk test, the evaluation of the wear volume follows the procedure describe in the ASTM G99, that is based on the analysis of the wear scar product on the pin and on the disc. The procedure is better described in Chapter 4.

2.5 Final comments

The present chapter focused on the analysis on the most important parameters influencing fretting wear on spline couplings. Basing the investigation on the Archard law, the parameters as contact pressure, sliding, wear coefficient and wear volume have been analysed.

The FEM analysis showed the necessity to realize micro geometries in splined couplings, in order to localize the damaged area in the middle zone of the teeth and to avoid pressure peaks at the extremities that may increase the surface damage. In addition to the microgeometries also the stiffness of the teeth is an important parameter in reducing the sliding, then the fretting wear.

Regarding the third important parameter of the Archard law, the wear coefficient, a procedure for its evaluation has been presented. It should be noted that the wear volume and the wear coefficient have been calculated on the basis of some hypothesis, as the elliptical shape of the footprint and the wear volume

as semi-ellipsoid volume. Given the difficulty on the individuation of the wear coefficient, the method can be used as a first approximation approach.

The prediction of the wear volume in mechanical components is complex. In this work a new method to theoretically calculate the wear volume on spline couplings has been presented. For the application of the method, based on the use of a pin-on-disk tribometer, the individuation of the "equivalent parameters" is required. Such parameters can be obtained by means of the numerical simulations and analytical models presented in the first paragraph.

2.6 References

[1]. Cuffaro, V., Curà, F., & Mura, A. (2014). Experimental investigation about surface damage in straight and crowned misaligned splined couplings. In *Key Engineering Materials* (Vol. 577, pp. 353-356). Trans Tech Publications.

[2]. DIN 5480-1. Involute splines based on reference diameters - Part 1: General.

[3]. Abaqus Theory Manual.

[4]. Giovannozzi, R. (1980). Costruzione di macchine, vol. I. *II, Bologna, Patron Editore*.

[5]. Tjernberg, A. (2001). Load distribution in the axial direction in a spline coupling. *Engineering Failure Analysis*, *8*(6), 557-570.

[6]. Barrot, A., Paredes, M., & Sartor, M. (2006). Determining both radial pressure distribution and torsional stiffness of involute spline couplings. *Proceedings of the Institution of Mechanical Engineers, Part C: Journal of Mechanical Engineering Science*, *220*(12), 1727-1738.

[7]. Ding, J., McColl, I. R., & Leen, S. B. (2007). The application of fretting wear modelling to a spline coupling. *Wear*, *262*(9-10), 1205-1216.

[8]. Hong, J., Talbot, D., & Kahraman, A. (2014). Load distribution analysis of clearance-fit spline joints using finite elements. *Mechanism and Machine Theory*, *74*, 42-57.

[9]. Hong, J., Talbot, D., & Kahraman, A. (2014). A semi-analytical load distribution model for side-fit involute splines. *Mechanism and Machine Theory*, *76*, 39-55.

[10]. Medina, S., & Olver, A. V. (2002). Regimes of contact in spline couplings. *Journal of tribology*, *124*(2), 351-357.

[11]. Curà, F., & Mura, A. (2018). Theoretical and numerical evaluation of tilting moment in crowned teeth splined couplings. *Meccanica*, *53*(1-2), 413-424.

[12]. Guo, Y., Keller, J., Moan, T., & Xing, Y. (2013). *Model fidelity study of dynamic transient loads in a wind turbine gearbox* (No. NREL/CP-5000-58414). National Renewable Energy Lab. (NREL), Golden, CO (United States).

3 Graphene as grease additive to improve tribological performances of spline couplings

3.1 Current status

Graphene has received a great interest by researchers in a wide field of applications. Referring to tribological aspects, graphene has been considered as an additive in lubricants, in order to reduce components friction and machine losses. Studies on both nanoscale and microscale demonstrated that applying graphene as lubricant, either solid or lubricant additive, allows to reduce considerably friction of steel, and then to drop wear by 3-4 orders of magnitude [1]. The early studies on graphene as solid lubricant were performed by Filleter et al. [2], demonstrating that a reduction of the thickness of the most common solid lubricant graphite to few layers allows a reduction of the friction coefficient. Some papers are available in literature about graphene utilized as additive in solids or liquid lubricants. In a form of modified graphene platelets (MGP), it has been used as a lubricant oil additive [3], showing an improving of oil performance in terms of reducing wear resistance. The reduction of friction and wear obtained using mineral oils formulated with graphene oxide (GO) nanosheets has been investigated in [4]. In [5] and [6] the effect of multilayer graphene nanosheets used as additive into respectively bentone grease and calcium grease has been analysed; a reduction of the friction coefficient due to the additive has been observed. Some other papers recently studied similar tribological aspects, exploring the possibility to reduce friction simply introducing graphene additives in classical lubricants [7]-[12].

Despite the big potential of graphene in this field, its use as a lubricant or a lubricant additive on macro-meso scale remains relatively unexplored [13]. In particular, the literature is lacking about specific applications of graphene added lubricants on mechanical systems.

Object of this chapter is to evaluate the possibility to use graphene as grease additive for spline couplings. Firstly, the Coefficient of Friction (CoF) of different compositions of grease-graphene compounds (grease added with Graphene Nano- Platelets) has been evaluated using a Pin-on-Disk Tribometer. Then, experimental tests on a dedicated test rig [14] have been performed in order to evaluate the effect of the grease-graphene compound on the CoF of the component.

3.2 Preliminary tribological tests with the grease compounds

3.2.1 Grease compounds analysed

Three different base greases have been used for the tests. The greases are commercial lubricants commonly used in mechanical components as spline couplings and bearings. Each grease is characterized by different chemical composition but all the three have excellent thermal stability within its operating temperature range.

Graphene Nano-Platelets (GNP) have been added to the base greases in order to evaluate its effect as lubricant additive. GNP have grade C-500 properties, characterized by 2 nm particles thickness, with a diameter less than 2 μm and average surface of 500 m^2/g. Different compounds of grease have been made using a Heidolph Torque Precision 400 homogenizer, then mixed for 30 min at room temperature in order to achieve uniformly dispersion of GNP into the grease.

For each grease the following compounds have been used to perform the tribological tests:

1. Grease A:
   a. Grease A - Pure
   b. Grease A + 0.5% GNP
   c. Grease A + 1% GNP
   d. Grease A + 5% GNP
2. Grease B:
   a. Grease B - Pure
   b. Grease B + 0.5% GNP
   c. Grease B + 1% GNP
   d. Grease B + 5% GNP
3. Grease C:
   a. Grease C - Pure
   b. Grease C + 0.5% GNP
   c. Grease C + 5% GNP

d. Grease C + 10% GNP

3.3 Tribometer tests: ball-on-disk

Coefficient of Friction (CoF) has been evaluated using a Pin-on-Disk Tribometer (TRB - Anton Paar) for a selected sliding distance, normal load and a linear sliding velocity. The pin has spherical shape: 6 mm diameter balls have been used for the test. The Pin-on-disk apparatus measures instantaneous values of CoF during the tests calculating at the end the average value. Table 3.1 displays the chosen parameters for the tests.

Base Material	% GNP	Load [N]	Linear Speed [m/s]	Sliding Distance [m]
Grease A	0.5 – 1 – 5	30	0.008 – 1.667	50 – 100
Grease B	0.5 – 1 – 5	30	0.008 – 1.667	50 – 100
Grease C	0.5 – 5 – 10	5	0.1	100

Table 3.1. Tests conditions used on the pin-on-disk tests for the greases.

For each compound three tests have been carried out. Both ball Specimen and disk specimen are made in C40 steel. During the tests temperature and humidity was constant and equal to 21°C and 40% respectively.

Figure 3.1 shows the tribometer apparatus with flat specimen covered by Pure Grease A (on the left) and specimen covered by Grease A + 0.5% GNP compound (on the right) installed.

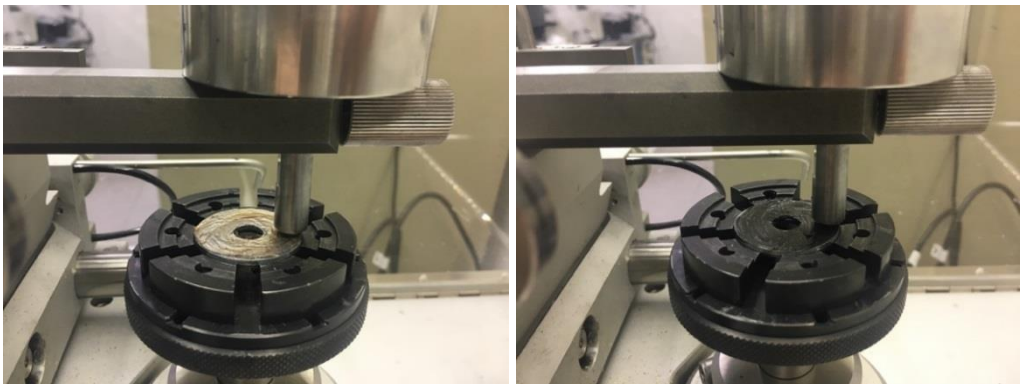

Figure 3.1. Pin-on-disk tests: specimen covered by Pure Grease (left) and specimen covered by Grease + 0.5% GNP.

3.3.1 Results

Figure 3.2, Figure 3.3 and Figure 3.4 shows an example of the results of the pin-on-disk tests for the three mixtures. The graph represents the trend of friction force F_F versus time. In all cases, an initial peak is observed: this could be due to the initial instability of the phenomenon. In fact, the very higher values of the CoF are recorded in the first test moments.

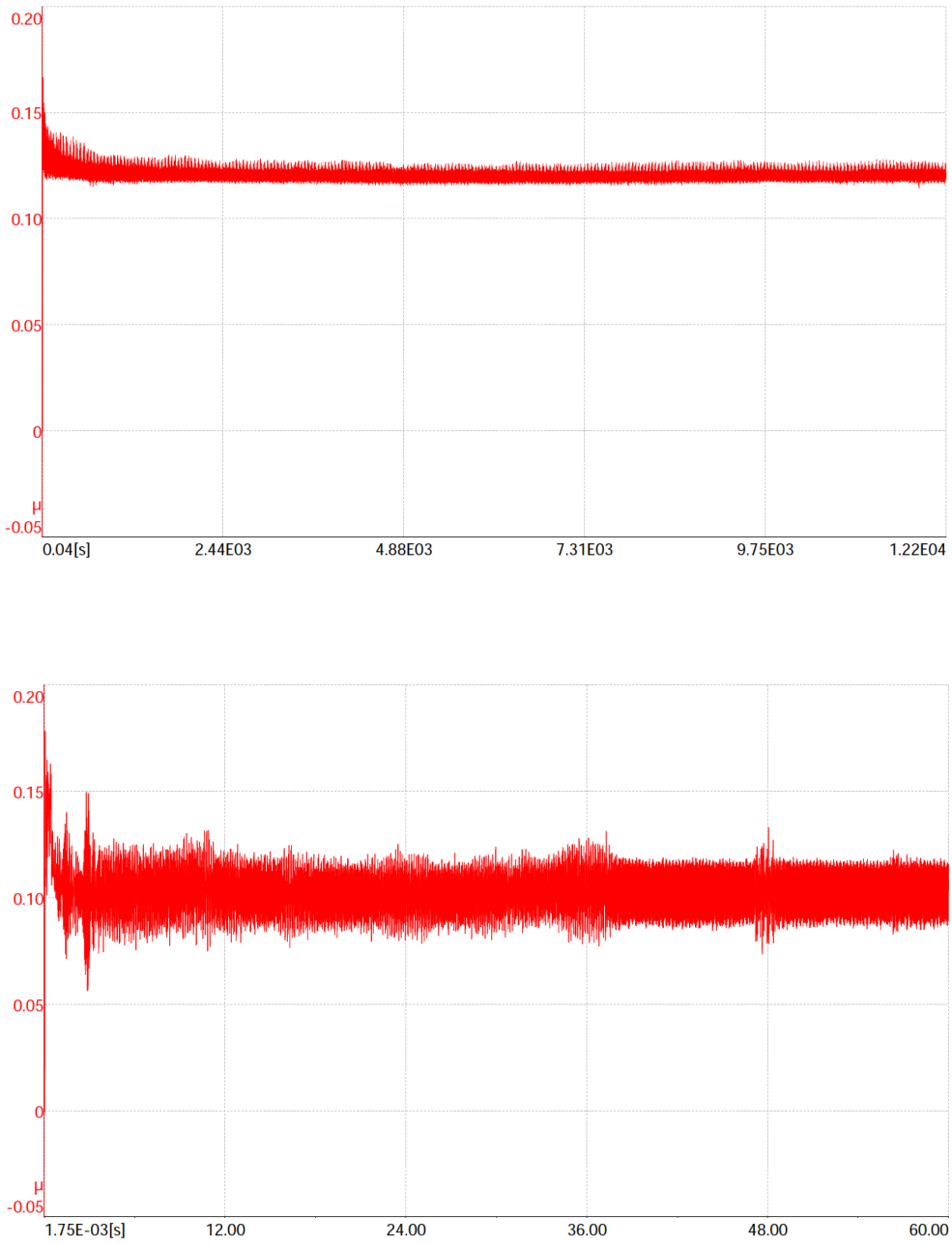

Figure 3.2. Example of CoF trend during the Pin-on-disk test: grease A pure at 0.008 m/s (up) and grease A pure at 1.667 m/s (down).

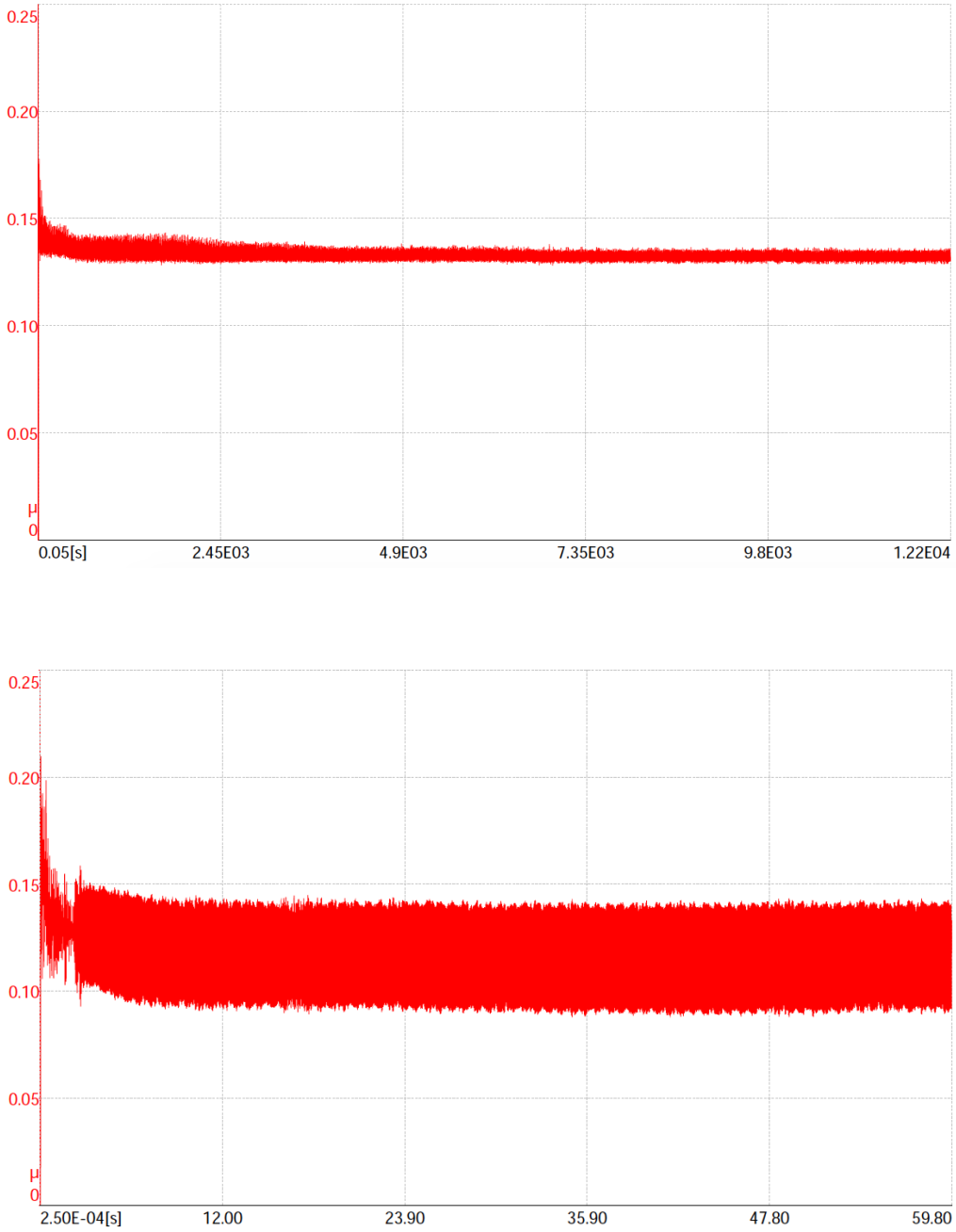

Figure 3.3. Example of CoF trend during the Pin-on-disk test: grease B pure at 0.008 m/s (up) and grease B pure at 1.667 m/s (down).

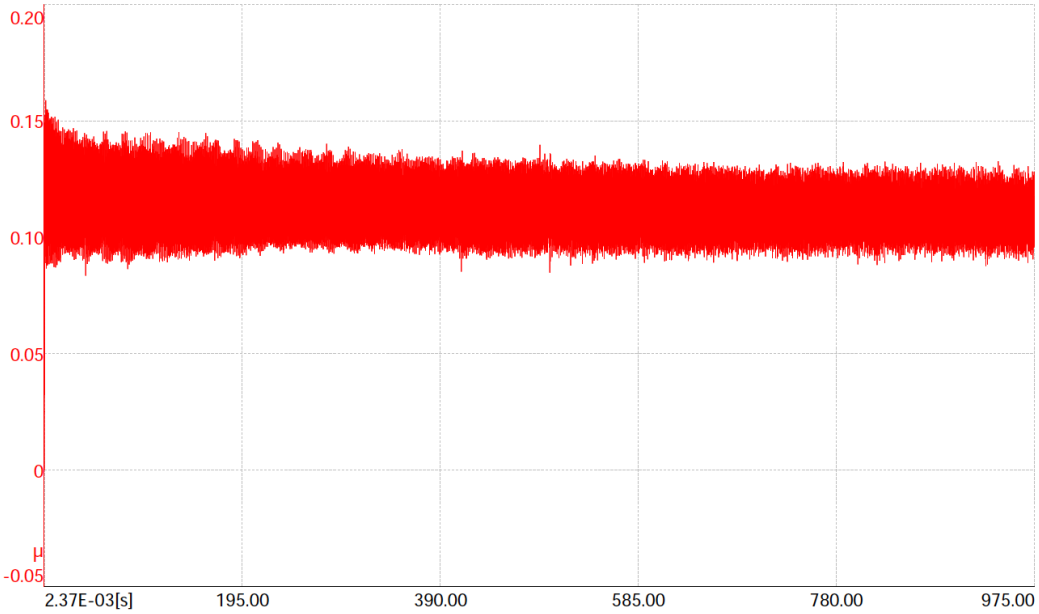

Figure 3.4. Example of CoF trend during the Pin-on-disk test: grease C pure at 8 mm/s.

Table 3.2 reports the results in terms of average CoF for each compound tested and the related standard deviation. For all configurations the low values of the standard deviation denote the small scattering between the same three tests executed. The diagrams in Figure 3.5, Figure 3.6 and Figure 3.7 better show the CoF values for each compound.

Grease A			
Linear Speed	Compound	CoF	St. Dev.
1.667 m/s	Grease A-Pure	0.112	0.007
	Grease A+0.5% GNP	0.116	0.004
	Grease A+1% GNP	0.105	0.04
	Grease A+5% GNP	0.116	0.01
0.008 m/s	Grease A-Pure	0.111	0.08
	Grease A+0.5% GNP	0.111	0.06
	Grease A+1% GNP	0.104	0.018
	Grease A+5% GNP	0.110	0.004

Grease B			
Linear Speed	Compound	CoF	St. Dev.
1.667 m/s	Grease B-Pure	0.116	0.002
	Grease B+0.5% GNP	0.126	0.006
	Grease B+1% GNP	0.119	0.005
	Grease B+5% GNP	0.122	0.006
0.008 m/s	Grease B-Pure	0.122	0.011

	Grease B+0.5% GNP	0.139	0.008
	Grease B+1% GNP	0.118	0.005
	Grease B+5% GNP	0.127	0.014

Grease C			
Linear Speed	Compound	CoF	St. Dev.
0.1 m/s	Grease C-Pure	0.130	0.020
	Grease B+0.5% GNP	0.111	0.010
	Grease B+5% GNP	0.097	0.006
	Grease B+10% GNP	0.114	0.001

Table 3.2. Pin-on-disk tests results: average CoF and standard deviation.

Regarding the Grease A (Figure 3.5), the values of CoF seems to be not strongly dependent from the linear speed of the tests: the CoF of the pure grease is equal to 0.111 and 0.112 in case of test velocity equal to 0.008 m/s and to 1.667 m/s respectively. Adding 0.5% of GNP to the grease A, the CoF remains the same (0.111 at 0.008 m/s) or even increases up to 0.116 for the tests at 1.667 m/s. A better results is registered for the "Grease A + 5% GNP" compound, for which the values of CoF decrease by 7%.

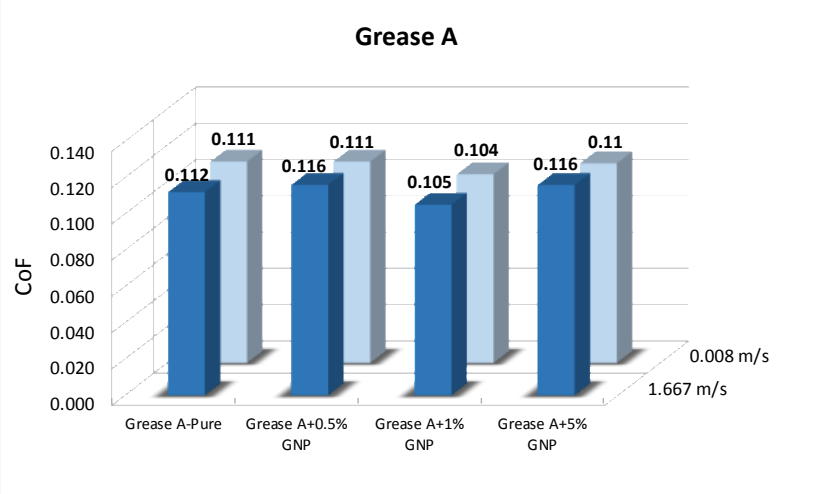

Figure 3.5. Average CoF values: Grease A.

For the Grease B (Figure 3.6) similar considerations to the grease A can be made. The linear velocity affects little the CoF trend. The best result is related to the "Grease B + 1% GNP" compound at 0.008 m/s: the CoF passes from 0.122 to 0.118, representing a reduction of only 3.3%. For the other compounds the results seem to be not promising.

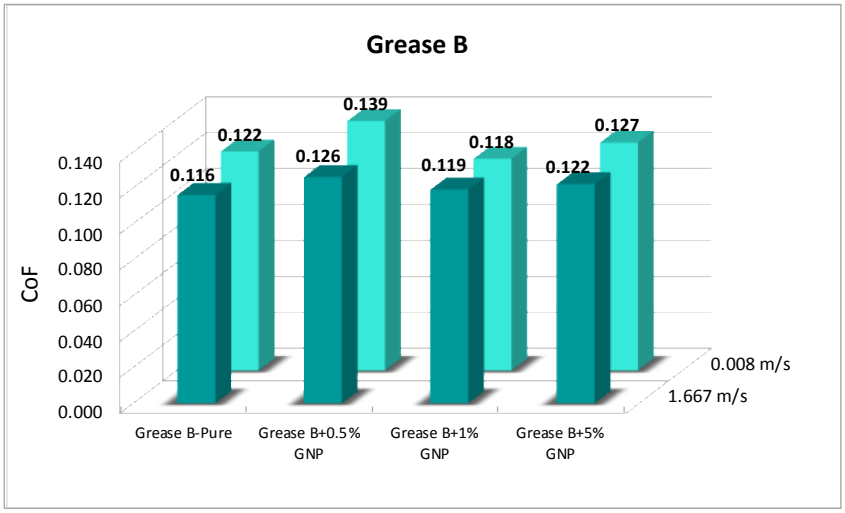

Figure 3.6. Average CoF values: Grease B.

The results of the Grease C, tested at a linear speed equal to 0.1 m/s, are shown in Figure 3.7. Starting from a value of 0.130 of the pure grease, the CoF decreases up to 0.111 when 0.5% of GNP is added. The best results are related to the "Grease C + 5% GNP" compound for which the CoF has a value of 0.097, representing a reduction of about 25%. A further addition of GNP (up to 10%) does not improve the results, but determine a little rise of the CoF value respect to the 5% GNP added. This could demonstrate that an optimal percentage of the additive exists and it has to be find within the 5% and 10%. Further experimental tests carried at different percentages of GNP within this range could provide the optimal value.

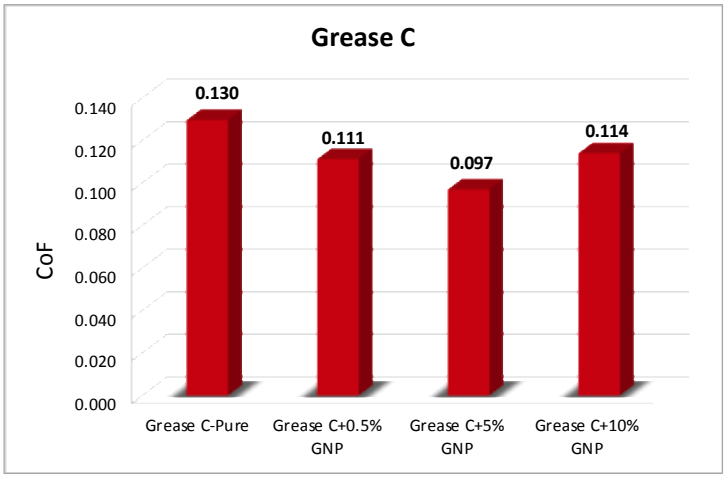

Figure 3.7. Average CoF values: Grease C.

Comparing the three greases, the Grease C presents the best results in terms of reduction of CoF. In general, all the three grease it is possible to affirm that an optimal value of GNP percentage exists and can be investigated.

3.4 Test bench experiments

Following the pin-on-disk results, a series of experimental tests on the mechanical component (the spline couplings) using similar grease compound have been carried out.

For the tests, a dedicated test rig has been used and the calculation of the CoF during the tests is based on the following considerations. In spline couplings the torque is transmitted thanks to the teeth of hub and shaft. In Figure 3.8 a generic scheme of spline couplings is shown. The presence of the torque T creates a tangential force F_{Ti} acting on each tooth pair. This tangential force F_{Ti} is the resultant of the contact pressure [15] and acts on the average contact radius r_a. The relation between the torque, the tangential force and the contact radius is the following:

$$T = \sum_{1}^{N} F_{Ti} \cdot r_a$$

where N is the number of engaging teeth.

The tangential force F_{Ti} acting on the surface of the teeth produces a friction force F_{Fi}; the two forces are linked by means the coefficient of friction μ as follows:

$$F_{Fi} = F_{Ti} \cdot \mu$$

Considering the whole component, the total friction force F_F acting on the spline coupling is equal to the sum of all the single friction forces F_{Fi} established on each teeth; the total force F_F is that necessary to move the shaft along the axis direction (Figure 3.8).

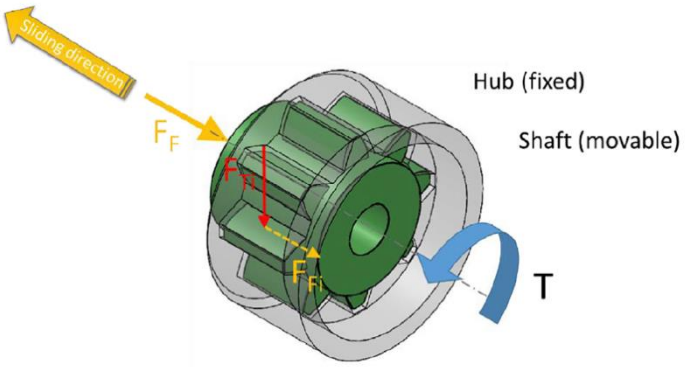

Figure 3.8. Spline coupling loading.

The calculation of the friction coefficient μ established between the teeth can be made starting from the value of the F_{Fi} (that can be measured) and applying the following equation:

$$F_{Fi} = \sum_{1}^{N} F_{Ti} \cdot \mu$$

3.4.1 Test bench description

The experimental tests on spline couplings have been carried out using a dedicated test rig. In Figure 3.9 and Figure 3.10 the relative scheme and picture are reported. On the test rig, the hub of the spline coupling is fixed on a rotating flange, connected to the fixed part of the system. The shaft of the spline coupling is connected to a skid mounted over two linear motion guides, in order to allow the linear motion of the part (the shaft).

The rotating shaft is connected to a bar where a force W can be produced by the positioning of a weight in the weight housing: the weight generates the force W necessary to produce the torque T that will acting the spline coupling. The load applied on the spline couplings can be varied by changing the weight applied. The maximum weight capability of the test rig corresponds to 50 kg, equal to a torque acting on the component equal to 63 Nm.

The skid is linked through a load cell to a screw jack activated by a gear motor that generates the linear motion and producing the sliding between the teeth. In fact, the screw jack pulls and pushes the shaft of the spline coupling with respect to the hub that is fixed; as a result, the load cell measures the force F_F needed to move the skid. Then, the coefficient of friction existing among the teeth in contact can be calculated as the ratio between the measured force F_F and the tangential force F_T generated by the torque.

The DC gearmotor mounted has a voltage equal to 24V, nominal torque equal to 4 Nm and maximum torque equal to 40 Nm. The rotational speed on the shaft at the out shaft is 35 rpm and the sliding velocity was set to 0.23 mm/s.

The load cell used is a Miniature Burster 8435 characterized by a measuring range of 1000 N. Data are acquired by a data acquisition board (NI USB-6210 National Instruments) with a sampling frequency of 50 Hz and collected by a dedicated software developed in LabVIEW environment.

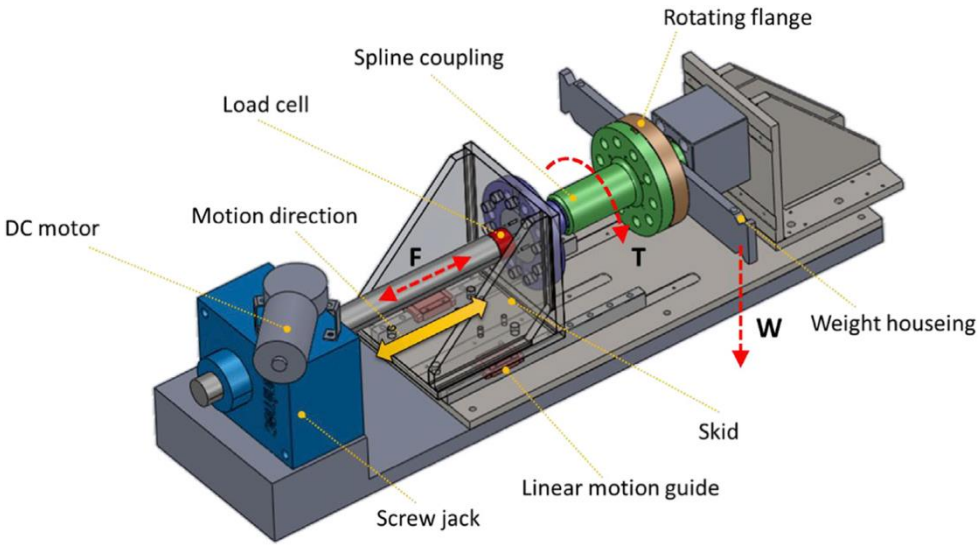

Figure 3.9. Scheme of the spline couplings test rig.

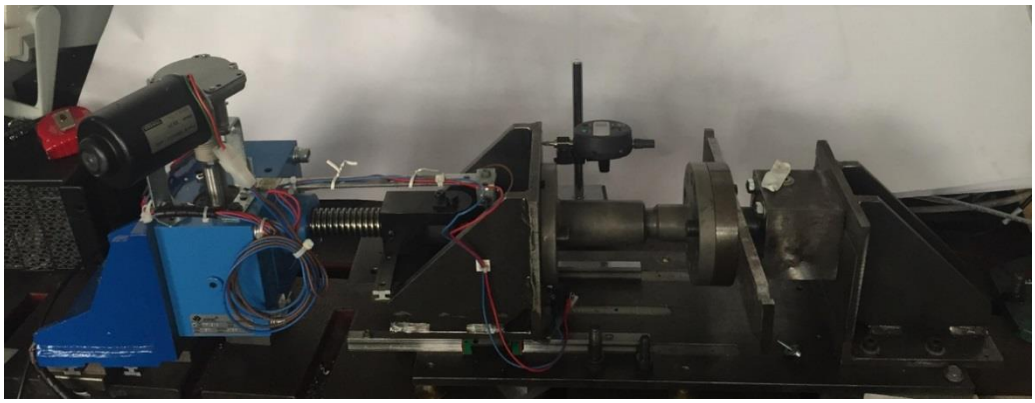

Figure 3.10. Picture of the spline couplings test rig.

3.4.2 Test conditions

For the experimental tests on the test rig different configurations have been applied. The reason of this is related to the need to describe as much as possible the real conditions at which the spline coupling can be subjected. The coefficient of friction calculated as the average of all different test performed will be more representative of the real working conditions. The spline couplings have been tested at different load levels: the load that will be applied between the teeth in contact has changed by varying the weight mounted on the weight housing.

Also the torque direction have been changed for the tests: in this way both of teeth side experienced the forces application. In Figure 3.11 a simple scheme of a section of the coupling is presented and the two possible torque directions are highlighted.

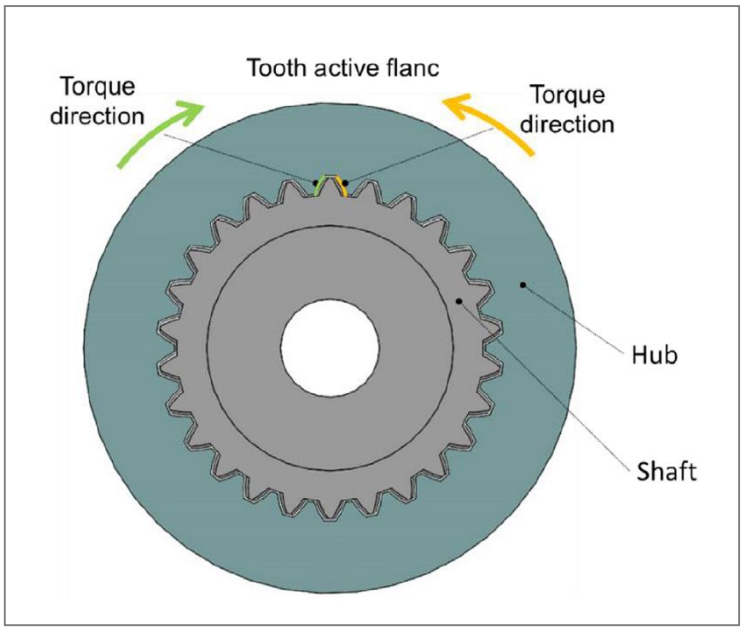

Figure 3.11. Representation of a transversal section of the coupling: both possible torque directions are highlighted.

Moreover, by rotating the shaft with respect to the hub different engaging position can be developed. In this case, all the test have been repeated by changing three times the angular position of the shaft respect to the hub: at 0°, 120° and 240°.

The last testing parameter considered is the direction of the teeth sliding: the friction force have been measured on both forwards and backwards direction.

Regarding the grease compound used to lubricate the teeth, based on the better results of the tribological tests the base grease used for the test rig experiments was the grease C. The commercial name is "SKF LGMT 2 grease" and the following five compounds have been analysed:

- Compound 1: grease only;
- Compound 2: grease + 0.5% GNP;
- Compound 3: grease + 1% GNP;
- Compound 4: grease + 5% GNP;
- Compound 5: grease + 10% GNP.

In Figure 3.12 the five mixture prepared for the test are shown.

Resuming all the possible configuration for the tests there are: three load level applied, two tooth sides tested, three engaging position considered and two sliding direction changed. In total, 36 kind of tests have been developed for each of the five lubricant compounds. For statistical concerns each test have been repeated three times. In total 540 tests have been performed.

Figure 3.12. The five compounds of grease and graphene used for the tests.

3.5 Test bench results

The graph of Figure 3.13 represents the trend of friction force F_F versus time. At the beginning of the test the force is zero, then the DC motor is activated push the foreword stroke then the force increases up to a steady state (when the velocity is constant), then after 8 mm stroke, the motion direction is automatically inverted and the force changes sign as now the motor pull backward the spline.

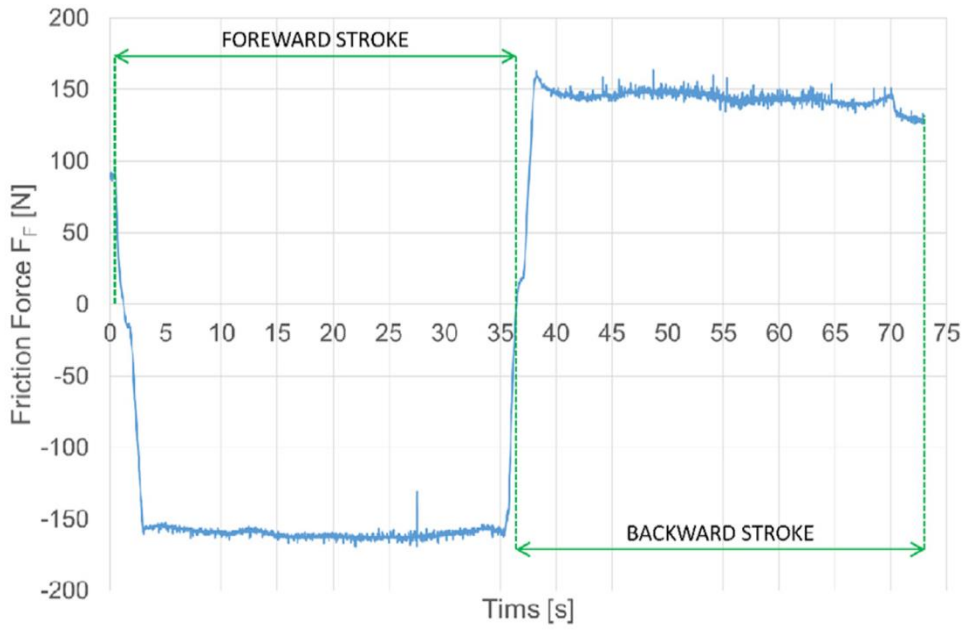

Figure 3.13. Example of data required from the test: friction force graph.

The value of the friction force F_F needed to the calculation of the coefficient of friction have been detected considering the stable part of the trend, and considering both the values related to the forward stroke and backward stroke.

Table 3.3, Table 3.4, Table 3.5, Table 3.6 and Table 3.7 show the results in terms of coefficient of friction (indicated as CoF) for each configuration of test performed. For every configuration the test have been repeated three times and the value of CoF reported is the average of the three tests. In particular, the tables report the results for each grease compound tested: in Table 3.3 the CoF values for the test performed with grease only are reported; Table 3.4, Table 3.5, Table 3.6 and Table 3.7 respectively show the results for the grease addictivated with 0.5%, 1%, 5% and 10% of Graphene Nano-Platelets (GNP).

In Table 3.8 a statistical analysis of all CoF values detected for each test is presented. Parameters as mean, standard deviation (StDev) and Confidence Intervals (CI) have been calculated on the basis of the one-way ANOVA.

Analysing in detail the results, the Compound 1 (pure grease) present a CoF equal to 0.141 that is considered as the value of reference. All the standard deviation values are low, indicating the good reliability of the results obtained in each tests. The intervals of confidence (CI) give a range of values probably containing the true mean of each group of measurements.

Compound 1							
Load [kg]	Side	0°		120°		240°	
		Onward	Back	Onward	Back	Onward	Back
5	left	0.143	0.143	0.144	0.138	0.145	0.141
	right	0.145	0.127	0.147	0.135	0.142	0.125
10	left	0.147	0.145	0.144	0.141	0.146	0.144
	right	0.149	0.132	0.150	0.135	0.141	0.130
15	left	0.144	0.144	0.146	0.142	0.148	0.145
	right	0.148	0.132	0.149	0.137	0.140	0.130

Table 3.3. CoF results of the tests performed using the Compound 1 (LGMT2).

Compound 2							
Load [kg]	Side	0°		120°		240°	
		Onward	Back	Onward	Back	Onward	Back
5	left	0.120	0.119	0.144	0.136	0.141	0.133
	right	0.12′	0.097	0.135	0.106	0.141	0.120
10	left	0.129	0.127	0.148	0.142	0.135	0.132
	right	0.121	0.115	0.136	0.116	0.135	0.123
15	left	0.133	0.132	0.146	0.142	0.138	0.135
	right	0.128	0.119	0.140	0.123	0.136	0.128

Table 3.4. CoF results of the tests performed using the Compound 2 (LGMT2 + 0.5% GNP).

Compound 3							
Load [kg]	Side	0°		120°		240°	
		Onward	Back	Onward	Back	Onward	Back
5	left	0.146	0.139	0.143	0.132	0.120	0.121
	right	0.123	0.122	0.147	0.126	0.119	0.108
10	left	0.135	0.132	0.134	0.131	0.128	0.125
	right	0.132	0.116	0.137	0.126	0.126	0.123
15	left	0.135	0.134	0.135	0.131	0.137	0.130
	right	0.131	0.118	0.136	0.127	0.131	0.122

Table 3.5. CoF results of the tests performed using the Compound 3 (LGMT2 + 1% GNP).

Compound 4							
Load [kg]	Side	0°		120°		240°	
		Onward	Back	Onward	Back	Onward	Back
5	left	0.132	0.114	0.143	0.117	0.117	0.117
	right	0.133	0.126	0.122	0.116	0.112	0.110
10	left	0.126	0.132	0.121	0.117	0.120	0.115
	right	0.125	0.119	0.127	0.122	0.116	0.110
15	left	0.125	0.134	0.127	0.118	0.122	0.115
	right	0.125	0.117	0.132	0.118	0.122	0.111

Table 3.6. CoF results of the tests performed using the Compound 4 (LGMT2 + 5% GNP).

Compound 5							
Load [kg]	Side	0°		120°		240°	
		Onward	Back	Onward	Back	Onward	Back
5	left	0.140	0.126	0.123	0.110	0.099	0.103
	right	0.136	0.118	0.125	0.104	0.101	0.095
10	left	0.131	0.125	0.118	0.115	0.113	0.110
	right	0.130	0.123	0.120	0.113	0.111	0.104
15	left	0.133	0.123	0.125	0.116	0.121	0.115
	right	0.131	0.122	0.123	0.114	0.120	0.108

Table 3.7. CoF results of the tests performed using the Compound 5 (LGMT2 + 10% GNP)

Test case	Number of tests	Mean	StDev	95% CI
Compound 1	108	0.141	0.006	(0.138; 0.144)
Compound 2	108	0.130	0.011	(0.127; 0.133)
Compound 3	108	0.129	0.008	(0.126; 0.132)
Compound 4	108	0.122	0.008	(0.119; 0.125)
Compound 5	108	0.118	0.011	(0.115; 0.121)

Table 3.8. Statistical analysis performed on the overall CoF results.

The general CoF trend for the five groups of tests is shown on Figure 3.14. On this figure the points highlighted correspond to the value of CoF found for each kind of test executed; they don't' represent the scattering of the results because of the different conditions at which the tests are conducted. In particular, observing each column of points, the points that have to be compared with each other are, for example, all the highest points at the different percentages, or the lowest points.

As can be seen, the CoF values decrease progressively with the adding of the Graphene Nano-Platelets. In particular, adding an amount of GNP equal to 0.5% (Compound 2) the CoF register a reduction equal to 7.8% (from 0.141 to 0.130). For the compound realized adding 1% of GNP (Compound 3) a further diminution of the CoF is registered: the value is equal to 0.129, corresponding to a difference of 8.5% respect to the Compound 1 (pure grease). Instead, the addition of 5% of GNP (Compound 4) leads to a reduction of the CoF equal to 13.5% respect to the pure grease (0.141 compared with 0.122). A further addition of GNP until the 10% (Compound 5) allows to register the maximum decrease of CoF that is equal to 16.3% (corresponding at a value of 0.118).

The positive effect on the reduction of the CoF addicting the grease with GNP could be due to the formation of a graphene protective layer on the surface of the specimen [5], [16].

Moreover, it is not to be excluded that the very thin nano platelets of graphene can produce a nano-ball bearings effect on the rubbing surfaces [6], [12].

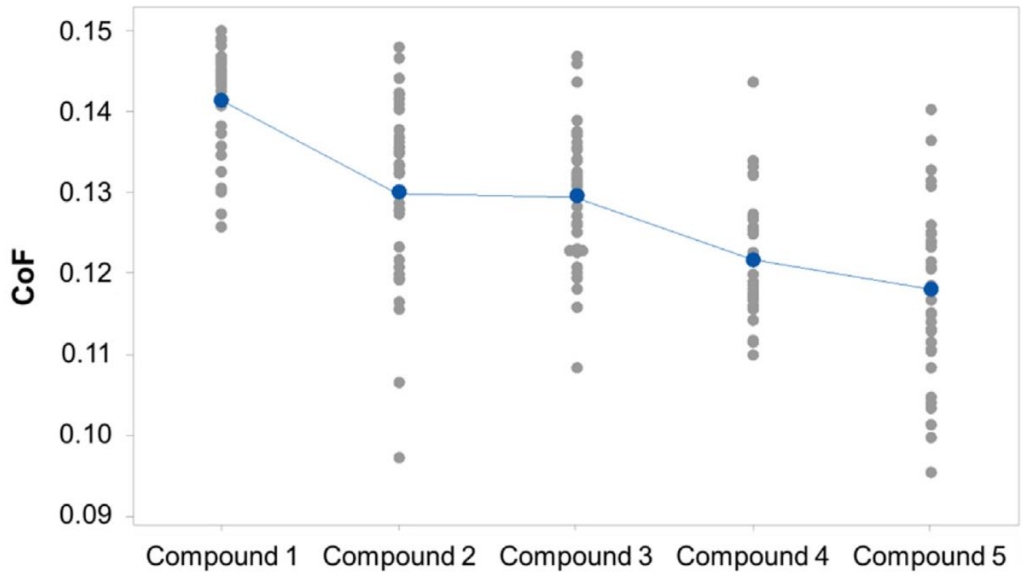

Figure 3.14. Plot of the CoF for each compound tested.

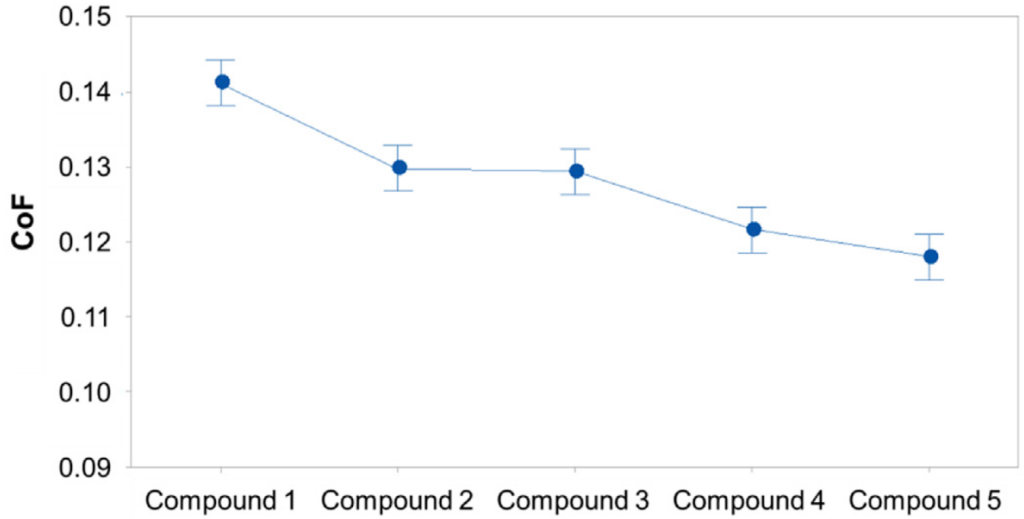

Figure 3.15. Plot of the CoF values for each compound tested with the scattering highlighted.

Comparing the CoF values obtained in both Pin-on-Disk and spline coupling tests (see Figure 3.16), it is possible to conclude that in the real application the CoF value are slightly bigger respect to the ones obtained by the Pin on Disk tests. This can be due to many causes, as for example the different contact regime and the different sliding velocities used in the two kind of tests. These parameters may affect the GNP distribution and the consequent effect on the tribological performance.

Finally, Figure 3.16 reports the comparison between CoF obtained in both Pin-on-Disk and spline coupling tests, in terms of CoF values.

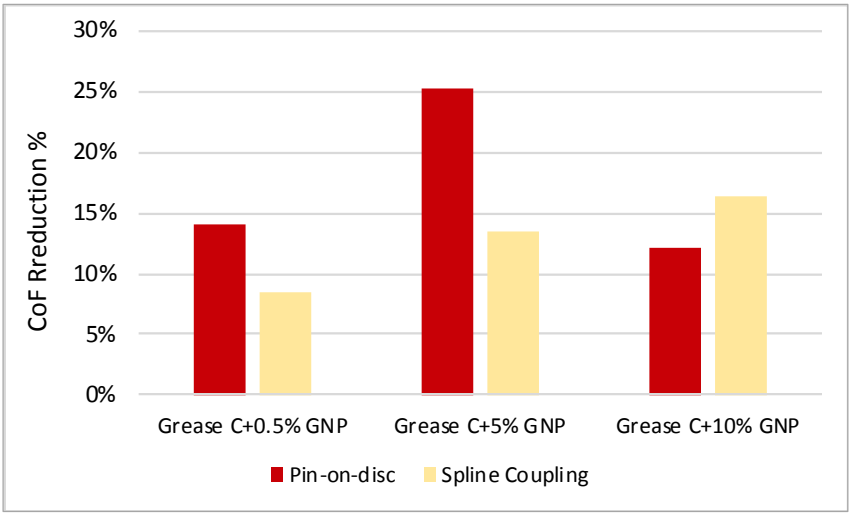

Figure 3.16. Comparison between CoF obtained in the Pin-on-Disk tests and spline coupling tests.

The results show that the GNP added to grease generally reduces the coefficient of friction, in both materials and components.

From the analysis of all results, it may be observed that the addition of GNP into the grease gives considerable benefits in terms of CoF reduction. Results also show that for the spline coupling the CoF reduces by increasing the percentage of GNP added into the grease, but the effect is different for the pin-on-disk tests, for which an optimal percentage of GNP exists.

3.6 Corrosion test

An important parameter in lubricants is the ability to attenuate or vice versa to increase the corrosion tendency of the mechanical components on which it is applied. In fact, the additive can improve the tribological properties of the lubricant/grease but it could worsen or improve other its properties, such as the corrosive characteristics. In many studies, other features are evaluated alongside the evaluation of the tribological effects of the additive [17], [18].

In this work, to assess the corrosivity of the grease with GNP a corrosion test has been carried out. The corrosivity test follows the ASTM D4048 [19]: the method involves the use of copper strips which are immersed in the grease, then left in an oven and subsequently examined according to a reference table.

Before the test all the samples have been mechanically cleaned and prepared with a dedicated wash solvent. The copper strips, insert within bakers full of grease, were placed inside the oven with a uniform temperature of 100 ° C for 24 hours without interruption (Figure 3.17).

At the end of the tests, the corrosiveness of the copper strips has been evaluated according to how they appearance agrees with the “Copper Strip Classification” guideline reported on the standard. The results are presented in Table 3.9.

Figure 3.17. Compounds inside the oven.

The addition of GNP to the Grease C causes a little increase of its corrosiveness passing from a "3b" grade to a "4a" grade for the 0.5% and 1% of GNP, arriving to "4b" grade in case of 5% and 10% of GNP added. On the basis of these results it can be stated that the corrosivity increases as the percentage added increases.

Grease	Classification	Designation	Description
Grease C Pure	3b	Dark Tarnish	Multicolored with red and green showing (peacock) but no grey
Grease C +0.5% GNP	4a	Corrosion	Transparent black, dark grey, or brown with peacock green barely showing
Grease C +1% GNP	4a	Corrosion	Transparent black, dark grey, or brown with peacock green barely showing
Grease C +5% GNP	4b	Corrosion	Graphite or lustreless black
Grease C +10% GNP	4b	Corrosion	Graphite or lustreless black

Table 3.9. Corrosion test results.

3.7 Final comments

The goal of this chapter was the investigation on the possibility to use Graphene Nano-Platelets (GNP) as grease additive. The purpose is the improvement of the lubricant properties in order to mitigate friction and wear on spline couplings. The reduction of the CoF, directly influencing the wear coefficient, can lead to less wear damage.

GNP has tested as additive for three different greases for spline couplings. A series of preliminary test on a pin-on-disk tribometer demonstrated the potentiality of GNP in reducing the CoF. In fact, the tests with the grease C with 5% of GNP registered a decrease of the CoF equal to 25%.

The grease C, that resulted that with the best results, have been used for the tests on the spline couplings. The experimental campaign have been conducted in a dedicated test rig and different configurations have been considered. The results of a total of 540 tests have been analysed by ANOVA analysis demonstrating its statistical reliability. Different percentages of GNP have been tested and the results demonstrating again the positive effect of GNP in reducing CoF. Using 10% of GNP the CoF reduces up to 16.3%.

3.8 References

[1]. Berman, D., Erdemir, A., & Sumant, A. V. (2013). Few layer graphene to reduce wear and friction on sliding steel surfaces. Carbon, 54, 454-459.

[2]. Filleter, T., McChesney, J. L., Bostwick, A., Rotenberg, E., Emtsev, K. V., Seyller, TH & Bennewitz, R. (2009). Friction and dissipation in epitaxial graphene films. Physical review letters, 102(8), 086102.

[3]. Lin, J., Wang, L., & Chen, G. (2011). Modification of graphene platelets and their tribological properties as a lubricant additive. Tribology letters, 41(1), 209-215.

[4]. Senatore, A., D'Agostino, V., Petrone, V., Ciambelli, P., & Sarno, M. (2013). Graphene oxide nanosheets as effective friction modifier for oil lubricant: materials, methods, and tribological results. ISRN Tribology, 2013.

[5]. Fan, X., Xia, Y., Wang, L., & Li, W. (2014). Multilayer graphene as a lubricating additive in bentone grease. Tribology Letters, 55(3), 455-464.

[6]. Kamel, B. M., Mohamed, A., El Sherbiny, M., Abed, K. A., & Abd-Rabou, M. (2017). Tribological properties of graphene nanosheets as an additive in calcium grease. Journal of Dispersion Science and Technology, 38(10), 1495-1500.

[7]. Yu, W., Xie, H., Chen, L., Zhu, Z., Zhao, J., & Zhang, Z. (2014). Graphene based silicone thermal greases. Physics Letters A, 378(3), 207-211.

[8]. Cheng, Z. L., & Qin, X. X. (2014). Study on friction performance of graphene-based semi-solid grease. Chinese Chemical Letters, 25(9), 1305-1307.

[9]. Liu, Y., Wang, X., Pan, G., & Luo, J. (2013). A comparative study between graphene oxide and diamond nanoparticles as water-based lubricating additives. Science China Technological Sciences, 56(1), 152-157.

[10]. Song, H. J., & Li, N. (2011). Frictional behaviour of oxide graphene nanosheets as water-base lubricant additive. Applied Physics A, 105(4), 827-832.

[11]. Fan, X., & Wang, L. (2015). High-performance lubricant additives based on modified graphene oxide by ionic liquids. Journal of colloid and interface science, 452, 98-108.

[12]. Fan, X., Li, W., Fu, H., Zhu, M., Wang, L., Cai, Z., ... & Li, H. (2017). Probing the function of solid nanoparticle structure under boundary lubrication. ACS Sustainable Chemistry & Engineering, 5(5), 4223-4233.

[13]. Berman, D., Erdemir, A., & Sumant, A. V. (2014). Graphene: a new emerging lubricant. Materials Today, 17(1), 31-42.

[14]. Mura, A., Curà, F., & Adamo, F. (2018). Evaluation of graphene grease compound as lubricant for spline couplings. Tribology International, 117, 162-167.

[15]. Cura, F., Mura, A., & Gravina, M. (2013). Load distribution in spline coupling teeth with parallel offset misalignment. Proceedings of the Institution of Mechanical Engineers, Part C: Journal of Mechanical Engineering Science, 227(10), 2195-2205.

[16]. Chu S, Jin Z, Xue Q. Study of the interaction between natural flake graphite and oil soluble additives. Tribology 1997; 17 (4):340–7.

[17]. Li J, Xu X, Wang Y, Ren T. Tribological studies on a novel borate ester containing benzothiazol-2-yl and disulfide groups as multifunctional additive. Tribol Int 2010;43:1048–53.

[18]. Zhan, W., Song, Y., Ren, T., & Liu, W. (2004). The tribological behaviour of some triazine–dithiocarbamate derivatives as additives in vegetable oil. Wear, 256(3-4), 268-274.

[19]. ASTM D4048 – Standard Test Method for Detection of Copper Corrosion from Lubricating Grease.

4 Graphene to decrease CoF and wear of steel

4.1 Current Status

In order to obtain good performances in sliding systems, it is very important to have low values of friction and wear. The improvement of the tribological behaviour of mechanical components is getting more and more importance for many researchers. In fact, friction and wear cause less efficiency, worse reliability and a shorter components life. It is possible to mitigate friction and wear applying liquid or solid lubricants at sliding contact interfaces.

When liquid lubricants cannot be used, as in some automotive components, aerospace systems and ultra-high vacuum technologies, solid lubricants, such as graphite, molybdenum disulfide (MoS2), and hexagonal boron nitride [1]-[3] are often used. The main issues about the use of solid lubricants regard their durability and their sensibility to environmental conditions, like the presence of humidity and oxygen [4]-[6]. Moreover, there are also several limitations in its application concerning the needed specific deposition techniques [7]. Considering what stated above, many recent research works are focused on the development of novel coating materials and deposition techniques.

Recently, several works analysed the use of graphene as an additive for lubricating oils/greases or as a solid lubricant [4], [8]. Graphene was discovered in 2004 [9] and it is a two-dimensional carbon material. It is very interesting for many applications for its exceptional mechanical and electrical properties. Moreover, several researchers, as Penkov et al [4], have highlighted that its properties are very well suited for tribological applications.

Many works highlighted how graphene can be very effective as lubricant oil additive: to improve oil performance and to reduce friction and wear is sufficient to add a little weight percentage of graphene [10] - [12]. Moreover, other studies have analysed the use of graphene as grease additive: the conclusions were that the presence of Graphene Nano-Platelets (GNP) into grease can enhance its tribological performances causing a reduction of both friction and wear of about 50% [13] - [15].

Furthermore, the use of graphene as coating of substrates to improve its tribological performances has been studied in several works. Different methods, including mechanical exfoliation [16], Chemical Vapor Deposition (CVD) [17] - [19], epitaxial growth [20], rod coating technique [21] and inkjet printing method [22] can be used to apply Graphene coatings.

In 2009, Filleter et al. [23] studied the effect of epitaxial graphene films on tribological properties of SiC substrates demonstrating that the presence of bilayer graphene leads to a reduction of friction by a factor of 2.

Kim et al. [24] demonstrated the feasibility of electrodynamic spraying process (ESP) covering method in the fabrication of Graphene Oxide Nanosheet (GONS) coatings; moreover, they highlighted its potentiality in reducing friction.

Berman et al. [8], [25] studied self-mated steel tribo-pairs in humid air and dry nitrogen with solution-processed graphene (SPG) in order to evaluate the friction behaviour; they found a decrease of friction and wear up to 3-4 and 6 order of magnitude respectively.

Kim et al. in 2011 [17] first studied the use of CVD-grown graphene films. Graphene grown on copper and nickel was used obtaining a decrease in adhesion and friction during micro-and nanoscale contact.

Established that graphene coatings improve the tribological performance in mechanical applications, it is useful to compare the performance of coated materials obtained by means of different coating techniques in order to identify their suitability for industrial application. In particular, clearly the most interesting coated material is steel as it is the most used material in mechanical applications.

In this work, C40 steel samples uncoated and coated with graphene applied by means of two different methods have been analysed and compared regarding their tribological performances. In several mechanical application the C40 steel is often used, therefore such material was considered as base material for the experiments. The two considered coating methods were CVD grown graphene on copper and then transferred on steel samples (TGC) and directly grown on steel graphene by CVD technique (DG); such last method has been applied considering growing times of both 5 and 10 minutes.

To evaluate the tribological performances of the samples, a series of ball-on-disc tests have been made. Based on such experiments, it was possible to examine the different graphene coated samples behaviours and to identify the best methods for mechanical applications in terms of friction and wear reduction.

4.2 Materials

The considered C40 steel specimens analysed in the experimental campaign have 10x10x4 mm dimensions. The preparation of such specimens was the following: firstly, the specimens have been grinded, obtaining an average Ra

roughness of 0.4 μm, and cleaned by sonication in acetone and then with water. Secondly, they were sonicated in Isopropyl Alcohol (IPA) in order to eliminate all the impurities and dirt. Finally, the surfaces have been coated.

4.3 Covering Processes

In order to cover the sample surfaces two different ting techniques have been used:

1) Direct Growth (DG) using CVD
2) Transferred Graphene Coating (TGC).

At the end of the tests, the results obtained have been analysed and compared to define the coating solution with the best tribological performance.

4.3.1 Direct Growth using CVD

The CVD technique [17], [18] used in the DG process, synthesizes large-area graphene directly on the specimen surface. The Ambient Pressure Chemical Vapor Deposition (APCVD) method has been utilized [19]. Firstly, the specimen is put into the CVD furnace (Figure 4.1) in which the temperature reaches 1000 °C in 30 min within a hydrogen environment obtained with 10 sccm of H2.

Temperature is maintained at 1000 °C for 30 min in order to conduct a pre-annealing process. When the mix of methane (10 sccm) and hydrogen (100 sccm) is put into the APCVD system, the graphene synthesis starts. Then, after growth, the specimens were quickly cooled to room temperature. Quality and quantity of the graphene layer coated surface can be influenced by the growing time [18], [19]. Therefore, two different direct growing times have been considered, 5 minutes (DG-5min) and 10 minutes (DG-10min), to highlight the effect of such parameter on the coated specimens' tribological performance.

Figure 4.1. LPCVD furnace; example with copper samples inside.

4.3.2 Transferred Graphene Coating

Following the LPCVD procedure [21], in the "Transferred Graphene Coating (TGC)" process the monolayer graphene film is grown on copper foil substrate.

In order to create a support layer for the graphene film, an EVA (Ethylene Vinyl Acetate) polymer coating is spin-coated on the graphene+copper foil and then dried in the oven at 80 °C. Then, by means of a copper etchant, the copper foil is removed.

The thin layer of graphene and EVA is then inserted in a deionized water bath, and subsequently transferred on the specimen surface. Follows the drying with N2 stream and oven baking at 80 °C for about 1 hour. Finally, the EVA is removed using xylene and the specimen is annealed to remove the remaining particles of EVA. This procedure is shown in Figure 4.2. By means of this procedure, it is possible to obtain graphene coating layers only 1 atom thick [26].

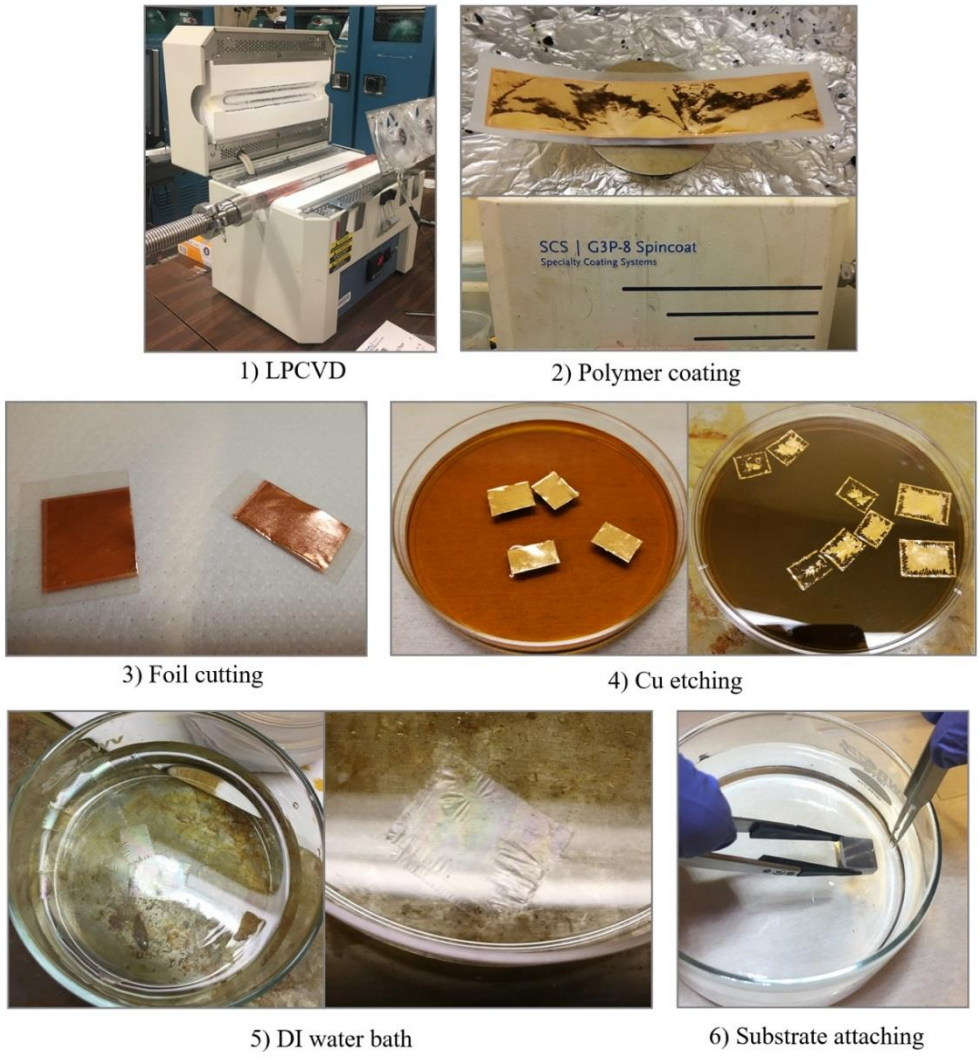

Figure 4.2. Transferred Graphene coating phases: (1) LPCVD, (2) Polymer coating, (3) Foil cutting, (4) Cu etching, (5) DI water bath, (6) Substrate attaching.

4.4 Experimental tests

A "TRB Anton Paar" Pin-on-Disk tribometer (Figure 4.3) has been used to carry out the tribological tests.

Considering the normal load on the disk, by means of the machine it is possible to measure the instantaneous friction force of the tribometer system and to obtain the Coefficient of Friction. Throughout the pin-on-disk test, a force of 5N has been applied, at a constant linear speed of 50 mm/s. It has been considered a total sliding distance of 100 m. A 100Cr6 steel ball with a radius of 3 mm has been used as a counterpart. The air temperature was 23°C while the humidity was 39%. Three tests for each specimen have been performed to give statistical meaningfulness at the experimental campaign. Wear race have been then measured by means of a profilometer (SM Metrology Systems PGS200), in order to calculate the worn material volume (according to ASTM G99 standard [27]).

Using a value of Young's modulus equal to 210 GPa, a Poisson's coefficient equal to 0.3, the maximum and mean hertzian contact pressure established between the pin and the specimen were respectively 710MPa and 470MPa.

During the tests the humidity and temperature have been monitored and the values was respectively 39% and 23°C. Each test have been repeated three times for statistical concerns.

The ASTM G99 [27] gives the guidelines to calculate the volume of material loss. The equation to use is the following:

$$V = \frac{\pi \cdot w^3 \cdot r}{6 \cdot R}$$

where w is the average wear race width (measured at three different points of the sample surface distant 120° each other); r is the radius of the wear track; R is the radius of the pin. Using a 2D profilometer (SM Metrology Systems PGS200) the wear track width has been scanned and measured.

In Table 4.1 the values of normal load and sliding speed used for the tests have been reported.

Sample Type	Number of test repetitions	Normal load [N]	Sliding speed [mm/s]
No coated	3	5	50
TGC	3	5	50
DG-5min	3	5	50
DG-10min	3	5	50

Table 4.1. Testing parameters set on the pin-on-disk tribometer.

For the sample covered by means the DG method a measurement of the Vickers Hardness (HV/0.3) have been carried out. The goal of the measurements

is to evaluate the effect of the DG covering process on the microstructure of the sample. As mentioned above, the DG process works at high temperature and the following cooling could be rapid. A micro hardness tester (Rupac Innovatest Nexus 4500) has been used; the measurement has been repeated 5 times and the average value of hardness have been calculated.

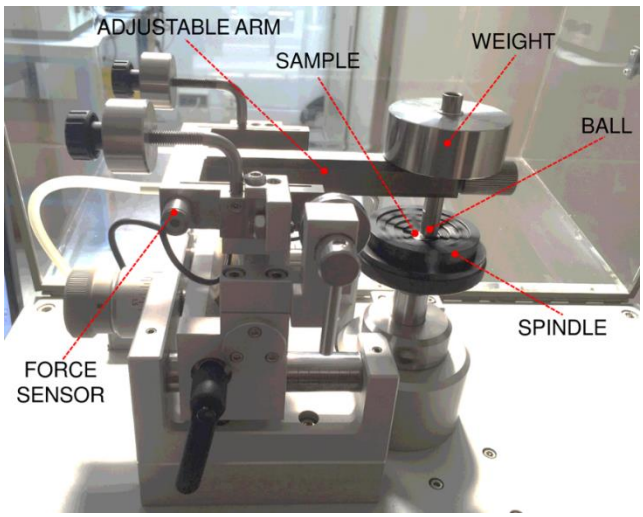

Figure 4.3. Principal components of the Pin-on-Disk tribometer (TRB Anton Paar).

4.5 Results

4.5.1 Hardness measurement

Figure 4.4 reports the results of the hardness detection. The Vickers hardness of the no coated sample (pure steel) is equal to 189 HV, while for the DG-5 min and DG-10 min the values are equal respectively to 187 HV and 164 HV. Then, the hardness of the samples covered using the 5 minutes process presents similar hardness of the pure steel. The DG-10 min specimen seems to be less hard than the original material, registering a reduction of the hardness of about 12%.The reason can be related to the high temperature process that lead to the decarburization of the sample surface [28].

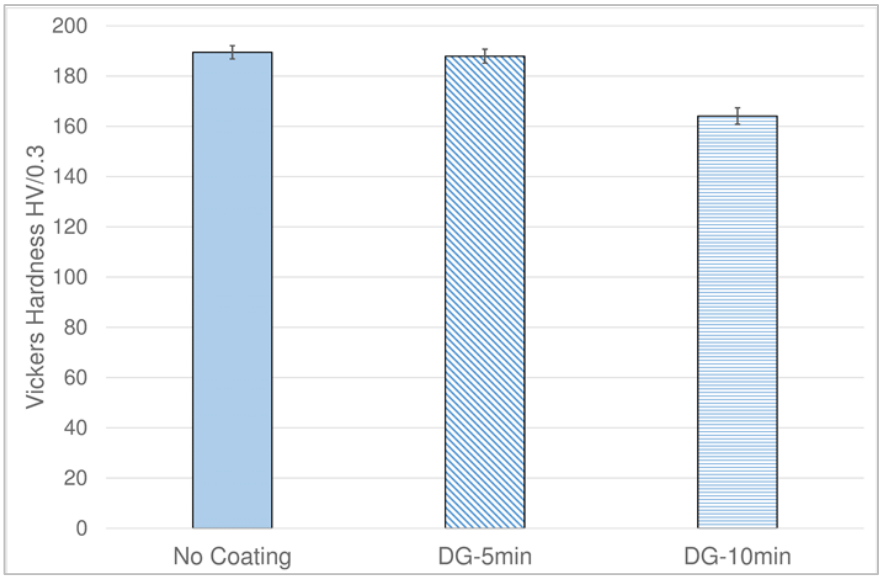

Figure 4.4. Values of Vickers Hardness for the no coating and DG covered samples.

4.5.2 Wear mechanisms

In order to analyse the wear mechanisms affecting the tested samples a series of SEM scans have been carried out. In Figure 4.5 an example of the SEM images detected for each kind of specimen have been reported. Two different magnifications have been used in order to highlights the wear track shape (smaller magnification) and the indications of the type of wear (higher magnification).

Comparing all the wear tracks of the specimens, the pure steel presents the bigger width. This indicates more material losing during the test, than a higher CoF established between the two surfaces (as the tribological results report).

In the Figure 4.5 (b) the wear scan of the TGC sample is reported: the surface is characterized by several scratch lines having the direction of the sliding. This kind of damage is typical of abrasive wear. Also the relative higher magnification (Figure 4.5 (b')) shows a very smooth surface, contrarily to the other three samples. The presence of abrasive wear could be the explanation of the better results in terms of CoF found for the TGC samples (see Figure 4.7).

Analysing the Figure 4.5 (c), the DG-5min sample seems to be principally affected by adhesive wear. The SEM scan, in fact, reveals a less defined wear track characterized by the presence of spallings and furrows. More in detail, the magnification of the DG-5min specimen (Figure 4.5 (c')) shows the presence of a crack. As descripted on the first chapter, the cracks are produced when fatigue wear mechanism occurring on the sliding system. The characteristics of the wear scar, the presence of both adhesive wear and fatigue wear can justify the poor effect on the reduction of the CoF reached by the DG-5min samples.

The wear scar of the DG-10 min (Figure 4.5 (d)) is characterized by more scuffing and plowing respect to the DG-5min ((Figure 4.5 (c)), but the

magnification of Figure 4.5 (d')) reveals also the presence of some furrow. If the scuffing and plowing are characteristic of abrasive wear, the furrow are typical of adhesive wear: in this case both phenomenon are coexisting.

For the DG-10 min (Figure 4.5 (d)) the degree of scuffing and plowing increases, but some furrow is still presents (highlighted by the magnification in indicating the coexistence of adhesive wear and abrasive wear.

By means of the SEM images is not so easy to comprehend if the graphene layer or a fraction of it still exist on the damaged surface. But, observing the higher magnifications of the coated specimens (Figure 4.5 (b'), (c') and (d')) the presence of several black zones can be noted. The black zones could be particles of graphene still present inside the wear track after the test.

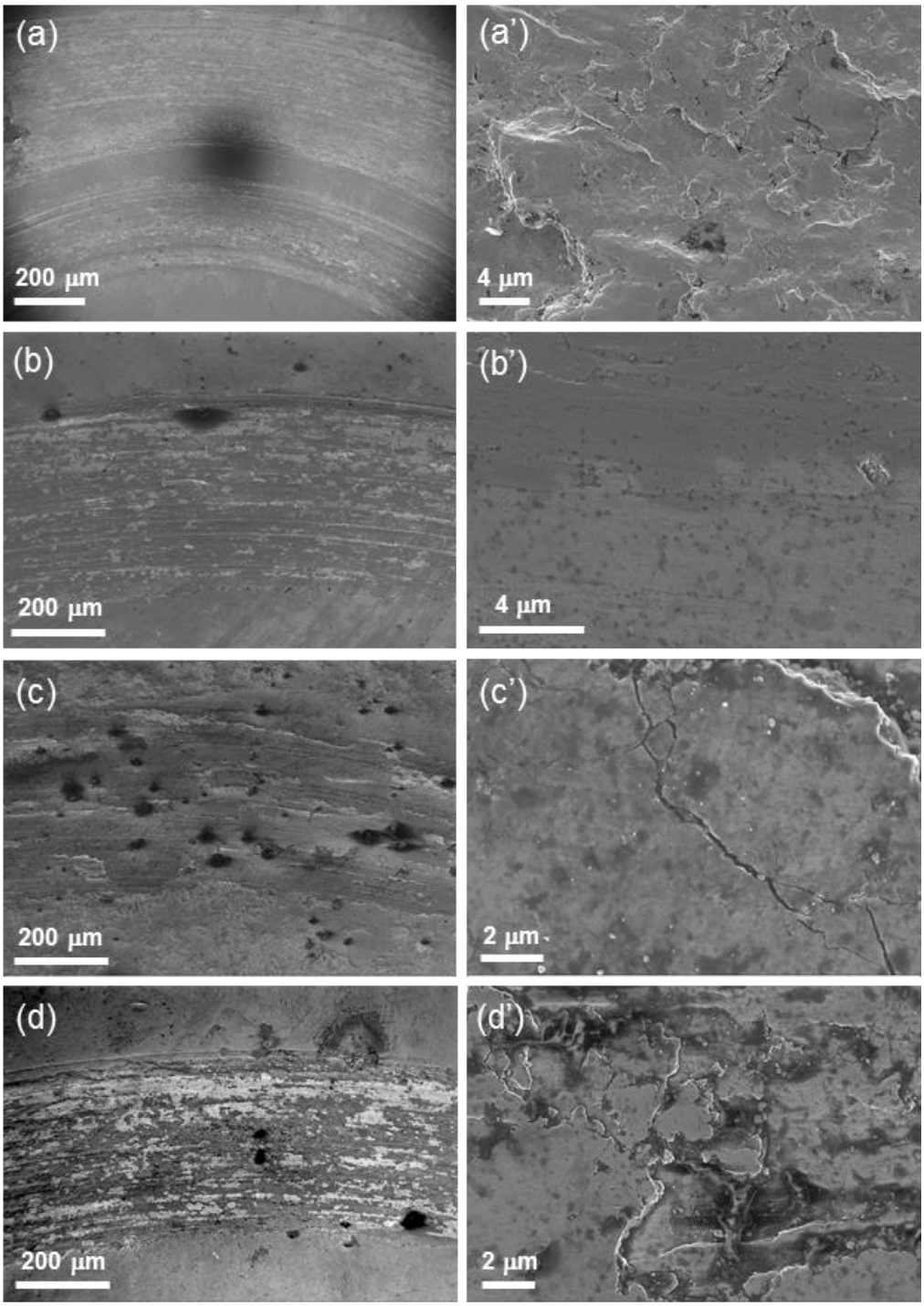

Figure 4.5. Wear tracks detected with the SEM: (a) Pure steel; (b) TGC; (c) DG-5min; (d) DG-10min; images marked with apex (') are the relative magnifications.

4.5.3 Coefficient of Friction

For all the samples tested the results in terms of coefficient of friction have been calculated considering the average CoF of each test (detected in 100 m of sliding distance).

In Figure 4.6 an example of the CoF trend in function of the sliding distance is shown. On the graph two zones are visible: a transient zone (where the CoF

vary due to the coating wear), and a steady state zone in which the CoF trend is practically constant. For the calculation of the CoF the values registered on the steady state zone have been used: the average represents the CoF result. Analysing the trend of CoF obtained, for each test the steady state zone has been identified starting from 40m of travelled distance (Figure 4.6).

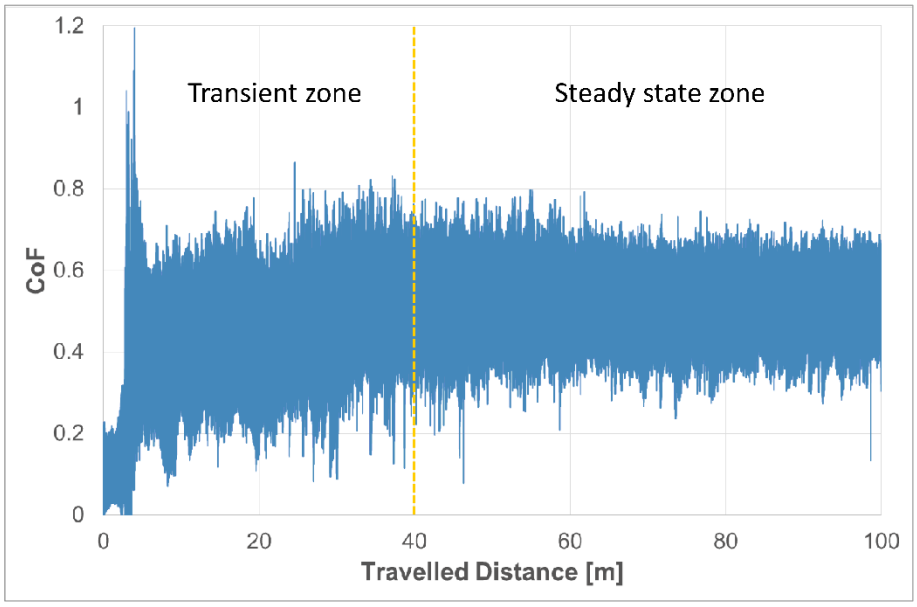

Figure 4.6. Example of CoF trend in function of the travelled distance (Test 1, DG-10min sample).

Figure 4.7 presents the average CoF values resulting from the tribometer tests. The values have been calculated as the average of three values.

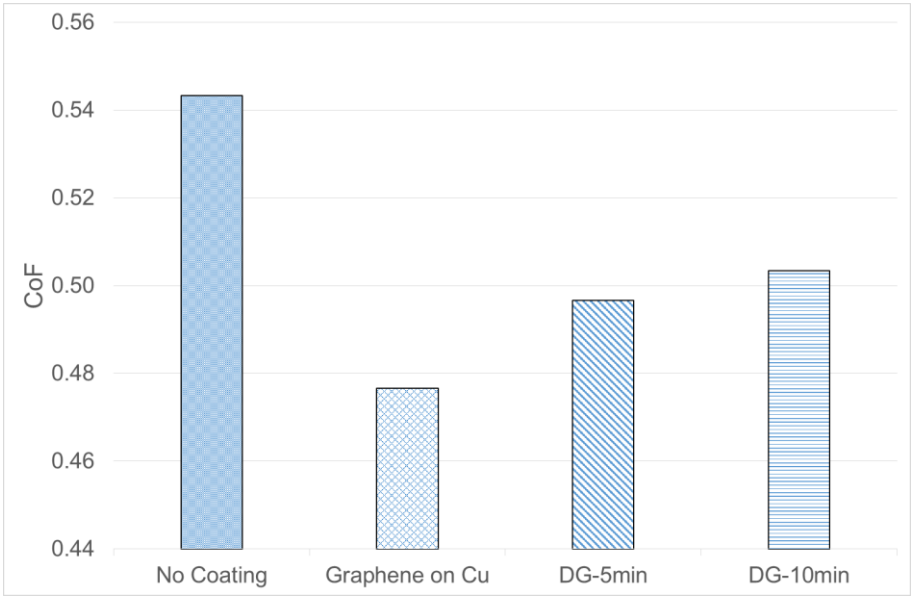

Figure 4.7. Values of CoF for the no coated and coated samples.

Generally, observing the results, the graphene coating seems to decrease the CoF of the samples. In particular, the specimen made by the transferred graphene coat (TGC) displays the best result, by diminishing the CoF of 12.5%. A CoF diminution is registered also for the samples with direct grown graphene, but less than the TGC one; in particular the DG-5 min samples presents a CoF reduction of 8.5%, while on the DG-10 min sample the decrease is equal to 7.5%. The samples covered by graphene could have a better behaviour thanks to the capability of the 2D material (as graphene) that inserted between contact surfaces allow the reduction of shear stresses and therefore reduction of CoF [8], [25], [29], [30]. It is important also to consider that the three coating methods presented lead to different coatings quality, in particular the TGC should develop a graphene layer with less adhesion respect to the DG graphene [17], [31], while, for the DG coatings the adhesion should be higher, but the growth time influences the number of defects on graphene coating [31]. As the results for the three methods in terms of CoF reduction are not so much different, it can be supposed that during the first laps, the graphene coating is broke, but small fragments of graphene remaining deposited on the sliding surfaces working as solid lubricant [32], [33].

4.5.4 Wear coefficient

In order to evaluate the effect of the graphene coatings on the wear strength of the samples, the specific wear rate k have been calculated. The calculation is based on the Archard law [34], as follow:

$$k = \frac{V}{S \cdot F}$$

In the equation V is worn volume at the end of the test, S is the total sliding distance and N is the applied load. For the calculation of the worm volume V the ASTM G99 [27] standard have been used: the track width of the sample surface at three different locations (at about 120° distance one from the other) have been measured, then the average of the three values have been calculated and inserted on apposite formula.

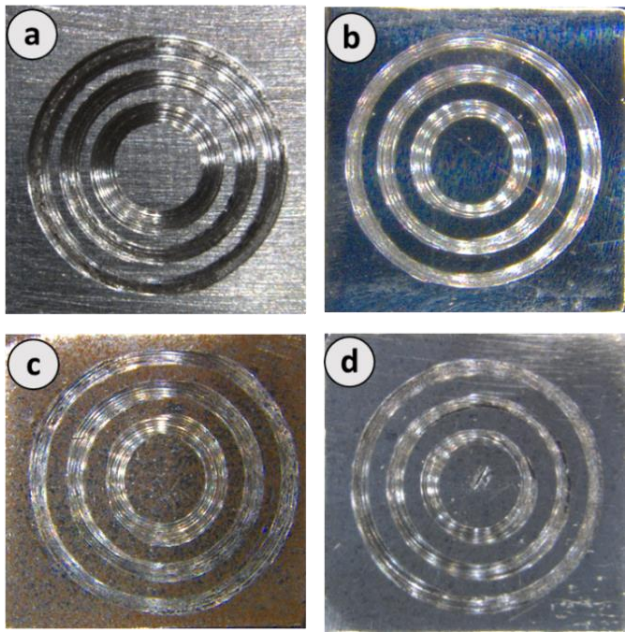

Figure 4.8. Optical images of the wear tracks: (a) no coating; (b) TGC; (c) DG-5min; (c) DG-10min.

In Figure 4.8 the optical images of the circular wear tracks after the tests are reported.

In Figure 4.9 the results in terms of specific wear rate for each kind of specimen is presented: the values are the average of three tests repeated at the same conditions.

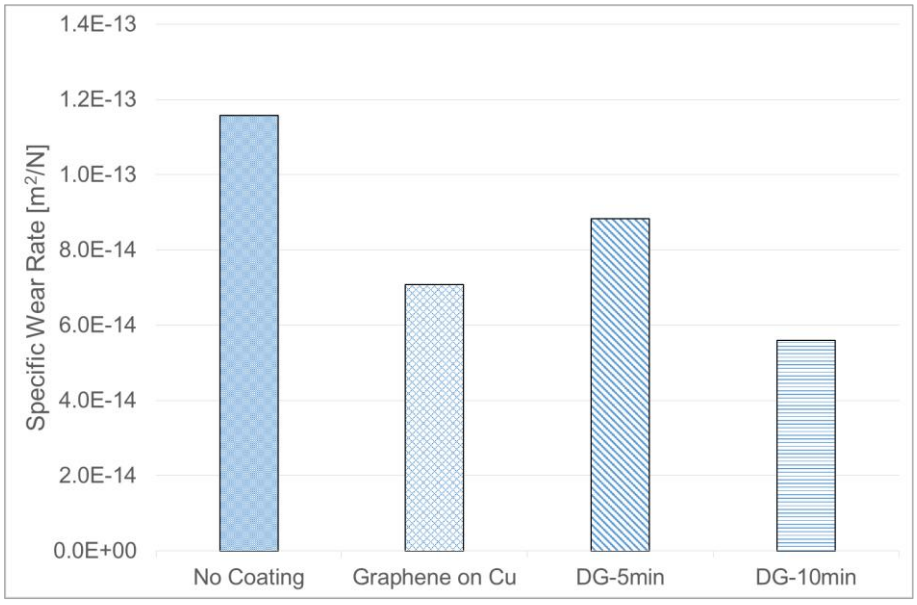

Figure 4.9: Specific wear rate.

The results shows that the coating method influences the specific wear rate of the sample. The best result is obtained for the DG-10 minutes sample: the reduction of k is equal to 52%. For the TGC samples the diminution is about

39%, while for the DG-5 minutes coating a reduction equal to 24% is observed. Maybe the less defects of the coating produced by a higher deposition time in case of DG-10 min sample, could explain its better results [31]; in fact, for the DG-5 minutes sample the results are not good as the DG-10 minutes sample; moreover, also the better coating adhesion of the DG-10 minutes coat could bring to better tribological performances [17]).

4.6 Final comments

In this chapter, the possibility to use graphene as solid lubricant for C40 steel have been investigated. On the study, the samples have been covered by graphene layer by using two different covering techniques. The first consists on the direct growth of grahene on the sample surface, while the second uses a layer of graphene previously grown on copper substrate and then transferred on the steel surface (here called TGC). For the DG method that uses a furnace for the growth, two different time of furnace pose have been considered: 5 minutes and 10 minutes. This, in order to evaluate the effect of the "cooking time" on the tribological properties of the samples.

The results of the ball-on-disc tests, analysed in terms of CoF and specific wear coefficient, show a general improvement thanks to the graphene coatings. In particular, the better CoF reduction is given by the TGC sample, while the smaller value of specific wear rate is given by the DG-10 minutes sample.

By means a surface analysis executed by Optical Microscope and SEM, the mechanism of wear affecting the different samples have been analysed. In particular, the samples without graphene show the typical signs of adhesive wear. Instead, the TGC is clearly affected by abrasive wear, while for the DG samples traces of both abrasive and adhesive wear are displayed.

The hardness measurement of the sample have been conducted in order to determine if the coating processes could affect the hardness of the sample: the results confirm that the DG technique (conducted by means a furnace) causes a decrease of the samples hardness, probably due to decarburization and grain growth.

Considering the overall results, the graphene coatings developed by the two technique presented seems to be promising in reducinf CoF and wear of C40 steel. Regarding the possibility to produce graphene coatings on a large-scale the DG methods should be more suitable than the TGC process on both technical and economic aspects.

On the idea to replace the actual lubricants nowadays used on the mechanical applications, the coatings presented could fulfil this function leading to the goal of machine weight reduction and environmental impact decrease.

4.7 References

[1]. Scharf, T. W., and S. V. Prasad. "Solid lubricants: a review." Journal of materials science 48.2 (2013): 511-531.
[2]. Erdemir, A., Solid Lubricants and Self-lubricating Films, in Handbook of Modern Tribology, (Ed. B. Bhushan) CRC Press 2001, 787 – 818.
[3]. Erdemir, A., and J-M. Martin. "New materials and coatings for superlubricity and near-wearless sliding." ASME/STLE 2007 International Joint Tribology Conference. American Society of Mechanical Engineers, 2007.
[4]. Penkov, O., Kim, H.J., Kim, H.J., Kim, D.E.: Tribology of graphene: a review. Int. J. Precis. Eng. Manuf. 15, 577–585 (2014)
[5]. Savage, Robert H. "Graphite lubrication." Journal of applied physics 19, no. 1 (1948): 1-10.
[6]. Arnell, R. D., Davies, P. B., Halling, J. & Whomes, T. L. Tribology - Principles and Design Applications 105±107 (Macmillan, London, 1991).
[7]. Berman, D., Erdemir A., and Sumant A. V. "Reduced wear and friction enabled by graphene layers on sliding steel surfaces in dry nitrogen." Carbon 59 (2013): 167-175.
[8]. Berman, D., Erdemir, A., Sumant, A.: Graphene: a new emerging lubricant. Mater. Today 17, 31–42 (2014)
[9]. Novoselov S. Graphene: materials in the flatland (Nobel Lecture). Angew Chem Int 2011; 50:6986–7002.
[10]. Lin J, Wang L, Chen G. Modification of graphene platelets and their tribological properties as a lubricant additive. Tribol Lett January 2011; 41:209–15.
[11]. Senatore A, D'Agostino V, Petrone V, Ciambelli P, Sarno M. Graphene oxide nanosheets as effective friction modifier oil lubricant: materials, methods, and tribological results. ISRN Tribol 2013: 1–9. Article ID 425809.
[12]. Dou X, Koltonow AR, He X, Jang HD, Wang Q, Chung YW, et al. Self-dispersed crumpled graphene balls in oil for friction and wear reduction. Proc Natl Acad Sci U. S. A 2016; 113(6): 1528–33. http://dx.doi.org/10.1073/pnas.1520994113.
[13]. Cheng Zhi-Lin, Qin Xi-Xi. Study on friction performance of graphene-based semisolid grease. Chin Chem Lett 2014; 25:1305–7.
[14]. Kamel Bahaa M, Mohamed Alaa, El Sherbiny M, Abed KA, Abd-Rabou M. Tribological properties of graphene nanosheets as an additive in calcium grease. J Dispersion Sci Technol 2017; 38 (10):1495–500.
[15]. Mura A, Curà F, Adamo F. Evaluation of graphene grease compound as lubricant for spline couplings. Tribology International. 2018 Jan 1; 117:162-7.
[16]. Singh, V., Joung, D., Zhai, L., Das, S., Khondaker, S.I., and Seal, S., "Graphene based Materials: Past, Present and Future," Progress in Materials Science, Vol. 56, No. 8, pp. 1178-1271, 2011.

[17]. Kim, K.S., Lee, H.J., Lee, C.G., Lee, S.K., Jang, H.U., Ahn, J.H.,Kim, J.H., Lee, H.J.: Chemical vapor deposition-grown graphene: the thinnest solid lubricant. ACS Nano 5, 5107–5114 (2011)
[18]. Shin, Yong Cheol, and Jing Kong. "Hydrogen-excluded graphene synthesis via atmospheric pressure chemical vapor deposition." Carbon 59 (2013): 439-447.
[19]. Wang, Haozhe, et al. "Low-Temperature Copper Bonding Strategy with Graphene Interlayer." ACS nano (2018).
[20]. Berger C, Song Z, Li X, Wu X, Brown N, Naud C, Mayou D, Li T, Hass J, Marchenkov AN, Conrad EH. Electronic confinement and coherence in patterned epitaxial graphene. Science. 2006 May 26; 312(5777):1191-6.
[21]. Dua, V., Surwade, S.P., Ammu, S., Agnihotra, S.R., Jain, S., Roberts, K.E., Park, S., Ruoff, R.S., Manohar, S.K.: All-organic vapor sensor using inkjet-printed reduced graphene oxide. Angew. Chem. 49, 1–5 (2010)
[22]. Wang, J., Liang, M., Fang, Y., Qiu, T., Zhang, J., Zhi, L.: Rodcoating: towards large-area fabrication of uniform reduced graphene oxide films for flexible touch screens. Adv. Mater. 24, 2874–2878 (2012)
[23]. Filleter, Tobin, et al. "Friction and dissipation in epitaxial graphene films." Physical review letters 102.8 (2009): 086102.
[24]. Kim, Hae-Jin, Oleksiy V. Penkov, and Dae-Eun Kim. "Tribological properties of graphene oxide nanosheet coating fabricated by using electrodynamic spraying process." Tribology Letters 57.3 (2015): 27.
[25]. Berman, Diana, Ali Erdemir, and Anirudha V. Sumant. "Few layer graphene to reduce wear and friction on sliding steel surfaces." Carbon 54 (2013): 454-459.
[26]. Jin-Yong Hong, Yong Cheol Shin, Ahmad Zubair, Yunwei Mao, Tomás Palacios, Mildred S. Dresselhaus, Sung Hyun Kim, Jing Kong, A Rational Strategy for Graphene Transfer on Substrates with Rough Features, Adv. Mater. 2016, 28, 2382–2392.
[27]. ASTM G99, Standard Test Method for Wear Testing with a Pin-on-Disk Apparatus, ASTM International, May 2017.
[28]. K. Adamaszek et al., "Decarburization and Hardness Changes in Carbon Steels Caused by High-Temperature Surface Oxidation in Ambient Air", Defect and Diffusion Forum, Vols. 194-199, pp. 1701-1706, 2001.
[29]. Pu, J., Wan, S., Zhao, W., Mo, Y., Zhang, X., and et al., "Preparation and Tribological Study of Functionalized Graphene-IL Nanocomposite Ultrathin Lubrication Films on Si Substrates," The Journal of Physical Chemistry C, Vol. 115, No. 27, pp. 13275-13284, 2011.
[30]. Liang H., Bu Y., Zhang J., Cao Z., and Liang A., "Graphene Oxide Film as Solid Lubricant," ACS Applied Materials Interfaces, Vol. 5, No. 13, pp. 6369-6375, 2013.
[31]. Won, M.S., Penkov, O.V., and Kin, D.E., Durability and degradation mechanism of graphene coatings on Cu substrates under dry coating sliding, Carbon, vol. 54, pp472-481, 2013.

[32]. Marchetto, D., Held, C., Hausen, F., Wählisch, F., Dienwiebel, M.,and Bennewitz, R., "Friction and Wear on Single-Layer Epitaxial Graphene in Multi-Asperity Contacts," Tribology Letters, Vol. 48, No. 1, pp. 77-82, 2012.
[33]. Mura, A., Adamo, F., Wang, H., Leong, W. S., Ji, X., & Kong, J. (2019). Investigation about tribological behavior of ABS and PC-ABS polymers coated with graphene. Tribology International, 134, 335-340.
[34]. J. F. Archard, Contact and Rubbing of Flat Surfaces, Journal of Applied Physics 24, 981 (1953); doi: 10.1063/1.1721448.

Conclusions

In this research the problems of friction and wear related to mechanical systems have been discussed. In particular, the work has been focused on the fretting wear affecting spline couplings. The phenomenon, happening between the teeth in contact, causes malfunction and loss of reliability in high-power transmissions.

After a preliminary description of the problem, the concepts of wear regime, wear mechanisms and wear models have been presented. Many authors investigated about the fretting wear occurring when sliding part are in contact presenting mathematical models and experimental tests. The main result comes from the Archard research: he developed the most common wear model, today used for many applications, called Archard model. The power of the model is the simplicity and adaptability to different conditions. According to the model, the wear volume produced in case of fretting depends directly on three parameters: contact pressure, sliding and wear coefficient.

The contact pressure strongly depends on the load applied between the teeth and on the design of the component. In order to find the most important microgeometry parameters that is important to consider to reduce the wear, a numerical model of crowned spline coupling have been developed. Basing on the geometry of the crowned spline couplings, the contact between the two engaging teeth can be modelled using the theory of Hertz. In this way, the numerical model has been validated applying the Hertzian theory finding good accordance. A series of numerical models characterized by different microgeometry have been developed. In particular, geometry parameters as crowning radius and tooth profile have been changed. The results highlight the importance to realize microgeometry in order to obtain to vary the values of contact pressure and its distribution.

Regarding the sliding occurring between the engaging teeth, it is found that there are two causes of them: the misalignment and the variable torque. The misalignment occurs when hub and shaft are not perfectly aligned: in this condition the contact point between the teeth move in harmonic way during the rotation of the component. Instead, the variable torque causes a different deflection of the teeth leading to sliding between the teeth in contact. For the

evaluation of the first contribute, an analytical approach has been presented based on kinematic considerations. While, the evaluation of the sliding due to the variable torque have been conducted by means the FEM model. Even using the numerical model, the influence of the tooth stiffness on the sliding have been estimated by changing the thickness. The results shown that changing the tooth thickness also the sliding varies.

The Wear volume is another parameter appearing on the Archard law. The computation of the amount of loss material on damaged spline couplings is a difficult issue. Then, basing on the Archard law, a method for the wear volume calculation has been presented. The method is based on the hypothesis that the wear scar is modelled as a fraction of ellipsoid. Starting from a 2D profilometer measure of the teeth profile and implementing mathematical considerations, the volume of the semi ellipsoid can be calculated by discretizing.

The realization of experimental tests on spline couplings in order to analyse how they are damaged depending on the work conditions is not even possible. The dimensions of the spline couplings for high power transmission, for example, make difficult the realization of apposite test rig. Following this consideration, a wear volume prediction method has been presented. The method is based on the use of a pin-on-disk tribometer in order to reproduce similar working conditions of a real spline couplings. Parameters as load, total distance travelled and sliding velocity can be calculated by means the Hertzian theory and the FEM model developed.

The last parameter involving on the Archard law is the wear coefficient. It depends on the material of the parts in contact but also on the lubrication conditions. In order to mitigate the fretting wear on spline couplings lubricated by grease an innovative additive has been presented: graphene. At first, a series of pin-on-disk tests have been conducted using different mixture of grease with graphene. The results have exhibited a good decrease on the coefficient of friction respect to the grease without graphene. Next, an experimental campaign conducted on spline couplings have been presented. For these experimental tests a dedicated test rig has been used. The results have demonstrated that using the graphene-grease compound the coefficient of friction established between the teeth in contact decreases, giving to less wear.

Finally, the possibility to use graphene as solid lubricant has been investigated. In fact, not in all application it is possible to apply liquid lubricant, and the use of solid lubricant is the only solution. A preliminary investigation about graphene cover on steel have been presented. Different covering process have been used and their difference on reduce the coefficient of friction have been evaluated. The experimental test conducted by means the pin-on-disk tribometer had done good results, confirming the high potentiality of graphene also as solid lubricant for steel. It is clear that the production methods presented in this work allow small-scale production and are suitable for the use in the research field. Future developments on methods that will allow large-scale

production at the industrial level would allow the use of graphene as lubricant in different sectors with more sustainable costs.